Geochemistry Geophysics Geosystems G3
AN ELECTRONIC JOURNAL OF THE EARTH SCIENCES
Published by AGU and the Geochemical Society

Article
Volume 8, Number 4
28 April 2007
Q04007, doi:10.1029/2006GC001443
ISSN: 1525-2027

Melt-mantle interactions beneath the Kamchatka arc: Evidence from ultramafic xenoliths from Shiveluch volcano

J. A. Bryant and G. M. Yogodzinski
Department of Geological Sciences, University of South Carolina, 701 Sumter Street, Columbia, South Carolina 29208 USA (jbryant@geol.sc.edu)

T. G. Churikova
Institute of Volcanology and Seismology Far East Division, Russian Academy of Sciences, 9 Piip Avenue, Petropavlovsk-Kamchatsky 683006, Russia

[1] Ultramafic xenoliths of spinel dunite, harzburgite, lherzolite, amphibole/phlogopite-bearing pyroxenite, and clinopyroxenite occur in andesitic pyroclastic debris from the 1964 eruption of Shiveluch volcano, Kamchatka. Peridotites have coarse/protogranular, porphyroclastic, and granuloblastic textures, abundant kink-banded olivine, and refractory mineral compositions with forsteritic olivine (Fo_{88-94}) and Cr-rich spinel (100*Cr/Cr + Al = 47–83). Orthopyroxene (opx) is also Mg-rich but occurs only as a fibrous mineral present along olivine grain boundaries, in monomineralic veins that crosscut coarse olivine, and in veins with amphibole and phlogopite that crosscut coarse-grained peridotites. Textural evidence and mineral compositions indicate that the peridotites and hydrous pyroxenites were replacive dunites that formed by melt-rock reactions involving the dissolution of pyroxene and precipitation of olivine. The fibrous opx and millimeter-scale veins of phlogopite, amphibole, and opx are interpreted as the autometasomatic products of hydrous magmas that were trapped in the uppermost mantle (<45 km). In this interpretation, opx was produced by reaction between late-stage, silica-rich, hydrous fluids/melts and olivine in the dunite protolith, and the millimeter-scale veins of phlogopite, amphibole, and opx are the volatile-enriched, deuteric products that were liberated during the final stages of magma crystallization. The absence of textural equilibrium suggests that the late-stage replacement process which produced the fibrous opx occurred shortly prior to the eruption that carried the xenoliths to the surface. On the basis of two-pyroxene thermometry and Ca-in-olivine barometry, the xenoliths equilibrated between 800 and 1000°C and 1.03 and 2.21 GPa. This implies that the xenoliths were carried from sub-Moho depths, a result consistent with geophysical estimates of crustal thickness. Olivine-opx-spinel equilibria indicate that the xenoliths are strongly oxidized with fO_2 from +1.4–2.6 log units above the fayalite-magnetite-quartz (ΔFMQ) buffer in peridotites, +1.7–2.3 ΔFMQ in hydrous pyroxenites, and +2.4–3.3 ΔFMQ in cumulate clinopyroxenites. High fO_2 in the peridotites is attributed to the melt-rock reactions that formed the dunite protolith. These results therefore suggest that interaction between oxidized melts and peridotite wall rock at shallow mantle depths plays a significant role in creating and modifying the uppermost mantle and deepest crust in some subduction settings.

Components: 10722 words, 12 figures, 6 tables.

Keywords: mantle; xenolith; peridotite; subduction; metasomatism; Kamchatka.

Index Terms: 3613 Mineralogy and Petrology: Subduction zone processes (1031, 3060, 8170, 8413); 3621 Mineralogy and Petrology: Mantle processes (1038); 3625 Mineralogy and Petrology: Petrography, microstructures, and textures.

Received 11 August 2006; **Revised** 18 January 2007; **Accepted** 31 January 2007; **Published** 28 April 2007.

Bryant, J. A., G. M. Yogodzinski, and T. G. Churikova (2007), Melt-mantle interactions beneath the Kamchatka arc: Evidence from ultramafic xenoliths from Shiveluch volcano, *Geochem. Geophys. Geosyst.*, *8*, Q04007, doi:10.1029/2006GC001443.

1. Introduction

[2] Melt generation at convergent plate boundaries is thought to be predominantly controlled by chemical fluxes of hydrous, volatile-bearing fluids or melts from the down-going oceanic plate to the upper mantle [*Kay*, 1980; *Perfit et al.*, 1980; *Ringwood*, 1974; *Tatsumi et al.*, 1986]. This process lowers the solidus of peridotite, and produces partial melt in the mantle wedge above the subducted plate and below the volcanic arc. The nature and composition of the subduction metasomatic flux and the source rock from which arc magmas are derived is most commonly addressed through geochemical studies of lavas that are erupted at the surface and seafloor sediments and oceanic crust that are carried to the mantle via subduction [e.g., *Hawkesworth et al.*, 1987; *Kay*, 1980; *Plank and Langmuir*, 1993]. An important limitation of this approach is that the composition of arc lavas is often significantly affected by differentiation within the crust upon which the volcano was built, thereby making it difficult in many cases to reconstruct mantle-level melting and enrichment histories.

[3] Another approach to understanding sub-arc mantle processes is through studies of ultramafic xenoliths from active subduction-related magmatic arcs, like those recognized in the Cascades [*Brandon and Draper*, 1996; *Draper*, 1992; *Ertan and Leeman*, 1996], Japan [*Takahashi*, 1980], Philippines [*Arai et al.*, 2004; *Maury et al.*, 1992; *Schiano et al.*, 1995], Mexico [*Blatter and Carmichael*, 1998], Papua New Guinea [*Franz et al.*, 2002; *McInnes et al.*, 2001], Lesser Antilles [*Parkinson et al.*, 2003], Aleutians [*Conrad and Kay*, 1984; *DeBari et al.*, 1987], and Kamchatka [*Arai et al.*, 2003; *Kepezhinskas and Defant*, 1996]. These studies are relatively rare, mainly due to the paucity of mantle xenoliths from modern arc volcanoes. Where arc xenoliths are found, they do, however, provide a unique opportunity to (1) directly observe fragments of the sub-arc mantle and deep crust and (2) investigate the physical conditions and geochemical processes of subduction zones in a way that is independent of observations of arc lavas.

[4] This paper provides new mineralogic and petrologic data on a collection of ultramafic xenoliths from Shiveluch volcano of the Kamchatka arc. The primary objective of this work is to infer the P-T-fO_2 conditions present in the upper mantle beneath Shiveluch volcano, and to constrain the petrological and geochemical processes that have acted there.

2. Xenolith Occurrence, Rock Types, and Mineralogy

[5] The xenoliths selected for this study were collected in 1998 and 2003 from Shiveluch volcano (SHX 98, SHX 03 sample IDs in Table 1), located on the Kamchatka Peninsula, near the junction of the Aleutian and Kamchatka subduction systems (Figure 1). Shiveluch is one of the largest and most explosively active volcanoes in Kamchatka, with eruption rates of 7×10^{10} kg per year through the Holocene [*Melekestsev et al.*, 1991; *Polyak and Melekestsev*, 1981]. Over twenty-five xenolith varieties have been recognized in the Holocene deposits from Shiveluch [*Koloskov and Khotin*, 1978; *Melekestsev et al.*, 1991]. The most common of these, including all of the xenoliths in this study (Table 1), are ultramafic in composition and were collected from within the pyroclastic debris of the explosive 1964 eruption, and on the surface of the associated debris avalanche.

Table 1. Classification and Modal Mineralogies for Shiveluch Xenoliths[a]

Sample	Rock Type	Group	% olv	% opx	% cpx	% spl	% amph	% phlog	Σr^2	Texture
SHX-03-01	harzburgite	peridotite	52.6	44.9	0.4	0.3	0.0	0.0	0.86	porphyroclastic
SHX-03-02	harzburgite	peridotite	62.0	27.8	0.8	1.1	7.0	0.0	0.21	porphyroclastic
SHX-03-03	harzburgite	peridotite	62.7	31.3	4.2	1.3	0.0	0.0	0.10	porphyroclastic
SHX-03-04	dunite	peridotite	90.0	6.5	0.0	3.0	0.0	0.0	0.09	coarse/protogranular
SHX-03-07	lherzolite	peridotite	57.9	26.8	12.0	2.6	0.0	0.0	0.07	porphyroclastic
SHX-03-08	harzburgite	peridotite	74.2	23.7	0.0	1.3	0.0	0.0	0.02	porphyroclastic
SHX-03-10	lherzolite	peridotite	53.4	38.0	5.5	3.4	0.0	0.0	0.05	porphyroclastic
SHX-03-12	harzburgite	peridotite	72.9	23.8	0.0	2.2	0.0	0.5	0.02	porphyroclastic
SHX-03-17	harzburgite	peridotite	78.9	15.4	0.0	3.0	0.8	2.1	0.09	coarse/protogranular
SHX-03-20	harzburgite	peridotite	87.5	10.0	0.0	1.7	0.0	0.0	0.09	coarse/protogranular
SHX-03-21	lherzolite	peridotite	54.0	22.6	21.9	1.5	0.0	0.0	0.22	porphyroclastic
SHX-03-24	harzburgite	peridotite	79.5	18.8	0.0	0.8	1.1	0.0	0.01	coarse/protogranular
SHX-03-26	harzburgite	peridotite	77.9	19.5	0.0	2.7	0.0	0.0	0.01	porphyroclastic
SHX-98-01	harzburgite	peridotite	86.8	10.8	1.0	1.3	0.0	0.0	0.06	coarse/protogranular
SHX-98-02	harzburgite	peridotite	77.7	20.3	0.0	1.6	0.0	0.0	0.16	granuloblastic
SHX-98-05	harzburgite	peridotite	83.2	13.6	0.0	1.5	0.0	0.0	0.94	porphyroclastic
SHX-98-06	harzburgite	peridotite	77.4	20.3	0.0	1.6	0.0	0.0	0.08	porphyroclastic
SHX-98-07	harzburgite	peridotite	74.7	20.1	2.6	2.2	0.0	0.0	0.16	porphyroclastic
SHX-98-16	harzburgite	peridotite	72.0	12.8	1.0	1.0	9.9	4.4	0.09	porphyroclastic
SHX-98-18	harzburgite	peridotite	57.4	37.0	0.0	2.9	2.4	2.6	0.09	porphyroclastic
SHX-98-PT	harzburgite	peridotite	78.6	20.7	0.0	0.7	0.0	0.0	0.10	granuloblastic
SHX-03-13	amph/olv websterite	hydrous pyroxenite	25.8	34.7	18.0	1.6	20.6	0.0	0.06	porphyroclastic
SHX-98-04	phlog/olv websterite	hydrous pyroxenite	30.4	54.2	6.0	1.5	0.0	8.6	0.19	porphyroclastic
SHX-98-12	amph/olv websterite	hydrous pyroxenite	6.0	72.3	15.3	1.8	4.3	0.0	0.12	porphyroclastic
SHX-03-19	olv websterite	clinpyroxenite	8.8	7.5	82.9	0.2	0.0	0.0	0.27	coarse-adcumulate
SHX-98-15	websterite	clinpyroxenite	0.8	15.8	80.0	2.1	0.0	0.0	0.08	coarse-adcumulate

[a]Modal mineralogies were calculated for each xenolith by fitting the average mineral composition of the major phases to the whole rock major element composition through a linear regression. The Σr^2 values indicate the calculated fit for each xenolith. Abbreviations: olv, olivine; opx, orthopyroxene; spl, spinel; cpx, clinopyroxene; amph, amphibole; phlog, phlogopite. Textures are from *Mercier and Nicolas* [1975] and *Harte* [1977]. Rock types are from *Streckeisen* [1979].

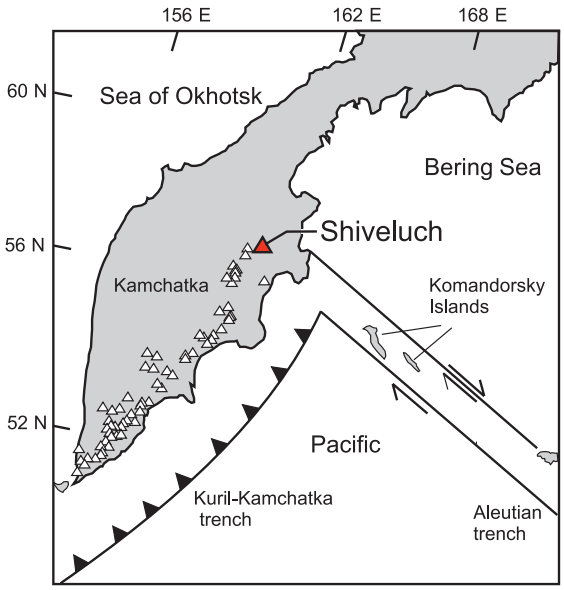

Figure 1. Location map of the North Pacific area showing the westernmost Aleutian and Komandorsky regions and the Kamchatka peninsula in the Russian Far East. Triangles indicate the locations of Quaternary volcanic centers in Kamchatka from the Smithsonian Global Volcanism database. The xenoliths were collected from Shiveluch Volcano, which is the northernmost active volcano of the Kurile-Kamchatka system.

[6] Ultramafic xenoliths from the 1964 eruption are mostly pale green in color, vary in size from 2–15 cm in average dimension, and are nearly always partially mantled by a 1–3 mm thick rim of hornblende (Figure 2a). Occasionally, the hornblende rims that surround the xenoliths are themselves mantled by a gray selvage of the vesiculated hornblende andesite host melt. Petrographic observations demonstrate that all of the xenoliths are pristine and free of alteration products such as serpentine, chlorite, or talc. The modal mineralogy for each of the twenty-six xenoliths included in this study was determined using a least squares linear regression to fit the average mineral compositions for the predominant mineral phases in each sample to the whole rock major element compositions (Table 1; Figure 3). On the basis of the calculated modes, spinel harzburgite (n = 17) is by far the most abundant xenolith rock type, with minor occurrences of spinel lherzolite (n = 3), dunite (n = 1), and websterite/pyroxenite (n = 5).

[7] The mineralogy of the peridotites is mostly olivine (53–90%) and opx (7–44%) with minor amounts of spinel (0.7–3.4%). Clinopyroxene (cpx) is rare in harzburgites with only one sample containing >1 wt% modal cpx. Phlogopite and amphibole are also minor hydrous phases (0–9.9%) occurring in veins and patches in six of the peridotites (e.g., Figure 2b).

[8] The pyroxenite xenoliths can be divided into two groups on the basis of their modal mineralogy. The first group we refer to as hydrous pyroxenites because they contain the hydrous minerals phlogopite (0–8.6%) and/or amphibole (0–21%) as well as abundant opx (35–72%). Olivine (6–30%), cpx (6–18%), and spinel (1.6–1.8%) are also present in the hydrous pyroxenites. The second group are clinopyroxenites containing ~80% cpx with minor amounts of olivine (0.8–8.9%), opx (7.4–15.8%),

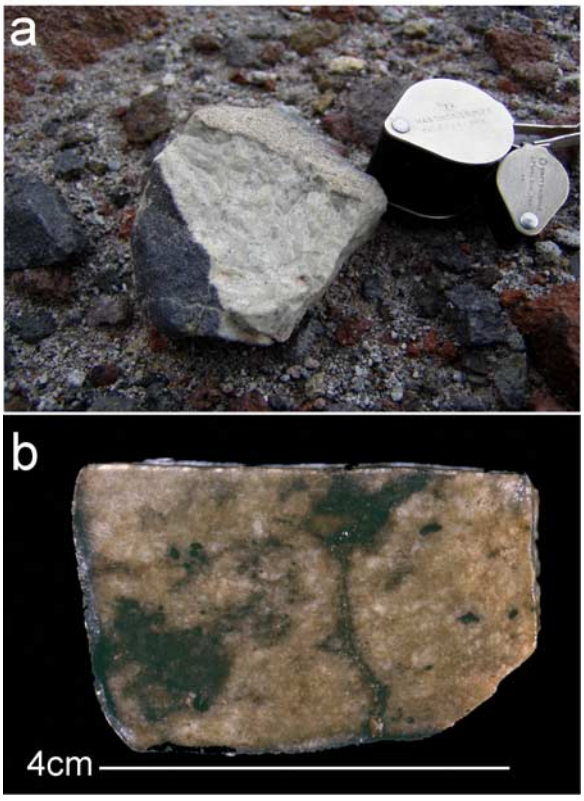

Figure 2. Photographs of Shiveluch xenoliths. Figure 2a shows a peridotite xenolith in place in the field as it was collected. The black surface of the sample (lower left) is a selvage of pargasitic hornblende. The xenolith is a typical pale green harzburgite, with small black specks of Cr-spinels. The smaller of the two hand lenses (for scale) is 1.5 cm in long dimension. Figure 2b is a thin section billet of a metasomatized peridotite, showing dark veins and patches of phlogopite-amphibole-opx. The long dimension of the xenolith is approximately 4 cm.

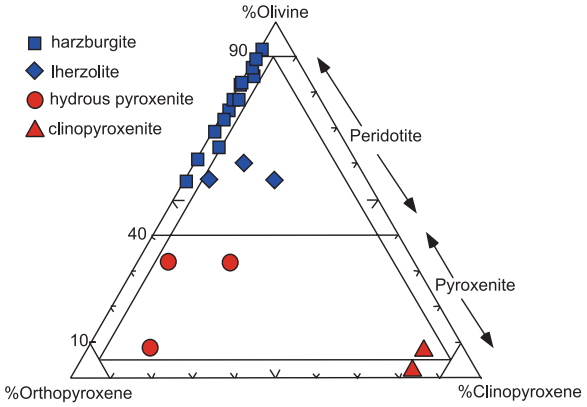

Figure 3. Mineral proportions (wt.%) in Shiveluch xenoliths plotted on the ternary classification diagram from *Streckeisen* [1979]. In addition to the mineral abundances shown here, the hydrous pyroxenites also contain up to 9% phlogopite or 21% amphibole. These data are from Table 1.

and spinel (0.1–2.1%), and are free of phlogopite and amphibole.

3. Textures and Petrography

3.1. Peridotites

[9] The peridotites show a wide range of deformation fabrics characterized by coarse equant/protogranular (Figure 4a), porphyroclastic (Figure 4b), and granuloblastic (Figure 4c) textures according to the nomenclature of *Harte* [1977] and *Mercier and Nicolas* [1975]. Coarse equant textures are restricted to samples with >78% modal olivine and olivine grain size is typically >2 mm (Figure 4a). In this texture, olivine commonly shows evidence of strain by the presence of kink-bands and subgrain structures [*Basu*, 1977; *Mercier and Nicolas*, 1975]. The most common texture observed in the peridotites is porphyroclastic, and these xenoliths have abundant coarse-grained olivine (>2 mm) surrounded mainly by a matrix of fine-grained opx (<1 mm), with minor occurrences of fine-grained olivine and cpx (Figure 4b). Clinopyroxene in the peridotite xenoliths is typically <300 μm and observable only by back-scattered electron microscopy (i.e., fine-grained section in Figure 4d).

[10] A significant feature of the peridotites is the absence of coarse opx and cpx and the abundance of fine-grained (<1 mm), fibrous opx (up to 45%), which forms in radiating aggregates along olivine grain boundaries or as monomineralic veins that crosscut olivine (Figures 4e and 4f and Figure 5). In some places the fibrous opx forms jagged and interpenetrating grain boundaries (on a scale of hundreds of microns) with the coarse olivine (Figure 4f). The most notable secondary texture in the peridotite xenoliths are the mm-scale veins of opx, phlogopite, and amphibole that crosscut coarse-grained olivine and the monomineralic veins of opx (Figure 6a). The best example of this texture is seen in a coarse equant harzburgite (SHX-03-17), where opx crystallizes on the outer edges of the vein and phlogopite, amphibole, and occasionally apatite form in the vein interior (Figures 6a and 6c). Phlogopite has also been recognized in patches that develop around spinel grain boundaries (Figure 6b).

3.2. Pyroxenites

[11] The hydrous pyroxenites contain up to 9% phlogopite, 21% amphibole, 72% opx, 30% olivine, and 18% cpx. Opx is fibrous and fine-grained, cpx and olivine are also relatively fine (<1 mm), and amphibole and phlogopite are developed primarily along cpx and spinel grain boundaries respectively (Figure 6d). The mineralogy and textures observed in these pyroxenites, especially with respect to the opx, is similar to that which is observed along olivine grain boundaries and in hydrous, mm-scale veins in the peridotites.

[12] The clinopyroxenites are coarse-grained xenoliths with approximately 80% cpx. These samples lack the deformation features that are common in the peridotites (i.e., kink-banding and grain-size reduction). Clinopyroxene grains are large (up to 4 mm; Figure 6e) and interlocking, similar to the adcumulate textures observed in layered igneous rock [e.g., *Wager and Brown*, 1967]. Orthopyroxene, olivine, and spinel are fine-grained (<1 mm) and present interstitially along cpx grain boundaries.

4. Analytical Methods

[13] Whole rock samples were sawn into two ~50 g slabs with a diamond wafer blade. One slab was used for thin sections and the other was crushed in a quartz-cleaned steel jaw crusher and ground in agate or aluminum ceramic grinding containers.

[14] Loss on ignition (LOI) was determined by heating ~4.0 grams of rock powder in quartz crucibles in a furnace for 16 hours at 900°C. Whole-rock major elements and some trace elements (Ni, Cr, V, Ba) were determined by XRF at the Washington State Geoanalytical Lab using a

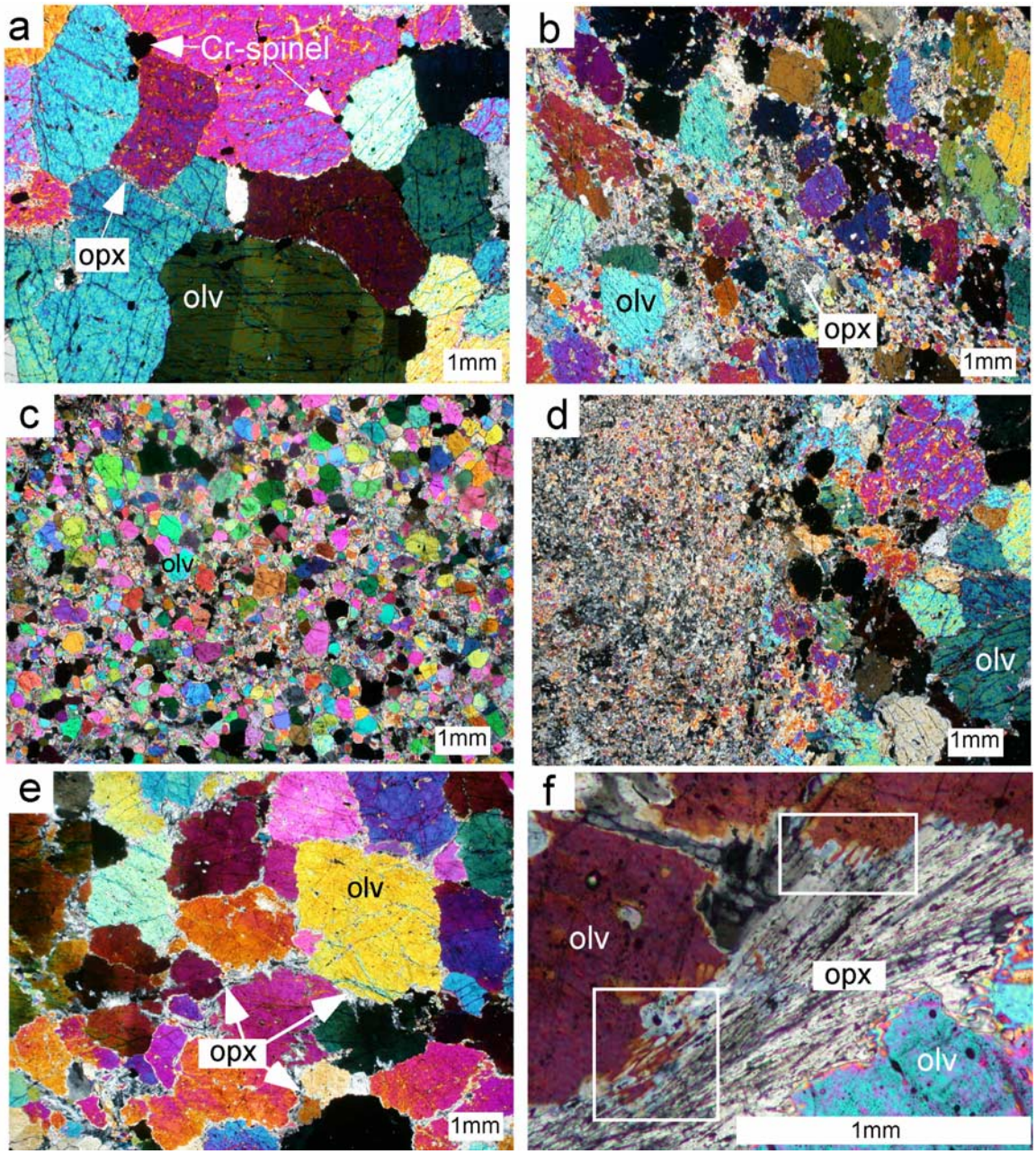

Figure 4. Cross-polarized photomicrographs of Shiveluch xenoliths: (a) coarse dunite showing kink-banding in olivine, (b) porphyroclastic harzburgite, (c) granuloblastic harzburgite, (d) spinel lherzolite showing a sharp contact between fine-grained and coarse-grained textures, (e) coarse harzburgite showing the growth of opx along olivine grain boundaries, and (f) fibrous opx adjacent to coarse olivine grains. Note the jagged and interpenetrating contact between fibrous opx and coarse olivine (white boxes), interpreted to indicate that opx was produced by replacement of olivine.

glass bead made from a mixture of 2.5 grams of rock powder, 1 gram of pure quartz, and 7 grams of Li-tetraborate flux. This quartz-dilution method is used to avoid crystallization of samples with greater than 40 wt% MgO. These data are reported on an anhydrous basis with analyses normalized to totals of 100% (Table 2).

[15] Mineral compositions were measured on a Cameca SX50 electron microprobe at the University of South Carolina, using an accelerating voltage of 15 kV and a beam current of 10 nA. Five different grains of each mineral phase present in the xenoliths were analyzed with count times of 30 s (Tables 3–5). X-ray maps were produced with an

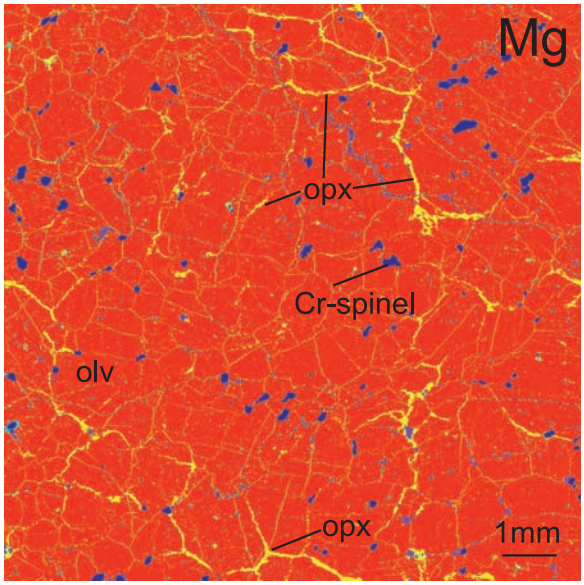

Figure 5. X-ray map of magnesium (Mg) of the coarse-grained dunite from Figure 4a (note similar scales). This image shows the distribution of fibrous opx along olivine grain boundaries and as monomineralic veins that crosscut coarse olivine.

accelerating voltage of 15 kV, a current of 200 nA, and a beam diameter of 5 μm. Calcium concentrations in olivine were determined using count times of 120 s for unknowns and 50 s for the diopside standard used for Ca (USNM-117733). The San Carlos olivine standard (SC/KA), which has a calcium concentration determined by isotope dilution [*Köhler and Brey*, 1990], was analyzed fourteen times during the analytical session, and was used as a check standard. The average calcium concentration in the check standard analyses from microprobe data (Ca = 523 ± 84 ppm 2-sigma) differed from the calcium determined by isotope dilution by only <2 ppm, or ~0.25% relative to the known value of 524 ppm (Table 6).

[16] Two spinel standards (KLB 8316 and VI314-5) with $Fe^{3+}/\sum Fe$ values that are known from ^{57}Fe Mössbauer spectroscopy [*Ionov and Wood*, 1992; *Wood and Virgo*, 1989] were analyzed twenty six times during a two-day microprobe session and were used as check standards to correct the $Fe^{3+}/\sum Fe$ of Shiveluch spinels. Determination of the $Fe^{3+}/\sum Fe$ values of these spinel standards and the Shiveluch spinels was calculated by converting the total FeO wt% from microprobe to Fe^{3+} and Fe^{2+} proportions assuming perfect M_3O_4 stoichiometry [*Droop*, 1987]. The average $Fe^{3+}/\sum Fe$ values of these spinel standards determined by microprobe differed from the know values from ^{57}Fe Mössbauer spectroscopy by −3%. The Shiveluch spinels measured during these sessions have been corrected on the basis of this error and were used to calculate fO_2 (Table 6).

5. Mineral Compositions

5.1. Peridotites

[17] The composition of olivine in the peridotites varies over only a narrow range with Fo_{90-94} in harzburgite and Fo_{88-89} in lherzolite (Table 3; Figure 7). Compositional variation within individual samples is also narrow. For example, core to rim line scans and X-ray maps on individual olivine grains coexisting with opx and cpx and adjacent to Cr-spinel show no significant change in Fo content or CaO wt% (Figure 8). Olivine compositions adjacent to opx, amphibole, and phlogopite veins are also homogeneous and similar to olivine in the interior of the xenoliths and away from veins (Tables 3 and 5).

[18] Spinel shows a wide range of Cr# (100*Cr/Cr + Al) and Mg# (100*Mg/Mg + Fe^{2+}) from 46.5–83.2 and 38.2–68.7 respectively (Table 3; Figure 7). In plots of forsterite content in olivine versus Cr# in spinel (Figure 7a), the Shiveluch peridotites fall within the olivine-spinel mantle array (OSMA) as defined by *Arai* [1994]. These compositions for olivine and spinel are refractory compared to abyssal and continental peridotites [*Dick and Bullen*, 1984; *Frey and Prinz*, 1978; *Luhr and Aranda-Gomez*, 1997], with high Fo content and high Cr#, similar to those reported for peridotites from the Izu-Bonin-Mariana arc [*Parkinson and Pearce*, 1998], peridotites from Avachinsky Volcano, Kamchatka [*Arai et al.*, 2003], and amphibole-bearing websterites from the Mexican arc [*Blatter and Carmichael*, 1998]. The Mg# of spinel is positively correlated with the Fo content in olivine (Figure 9b). The $Fe^{3+}/\sum Fe$ of spinel in the peridotites and hydrous pyroxenites is relatively low, with $Fe^{3+}/\sum Fe$ from 0.23–0.54, compared to magnetite in the clinopyroxenites with $Fe^{3+}/\sum Fe$ from 0.65–0.71 (Table 6; Figure 7c).

[19] Orthopyroxene compositions are also relatively homogeneous in peridotites with Mg# (100*Mg/Mg + Fe^{2+}) from 89.2–98.6, CaO <1 wt%, and Al_2O_3 <2 wt% (Figure 9), regardless of whether it has crystallized within amphibole and phlogopite veins or along olivine grain boundaries (Tables 3

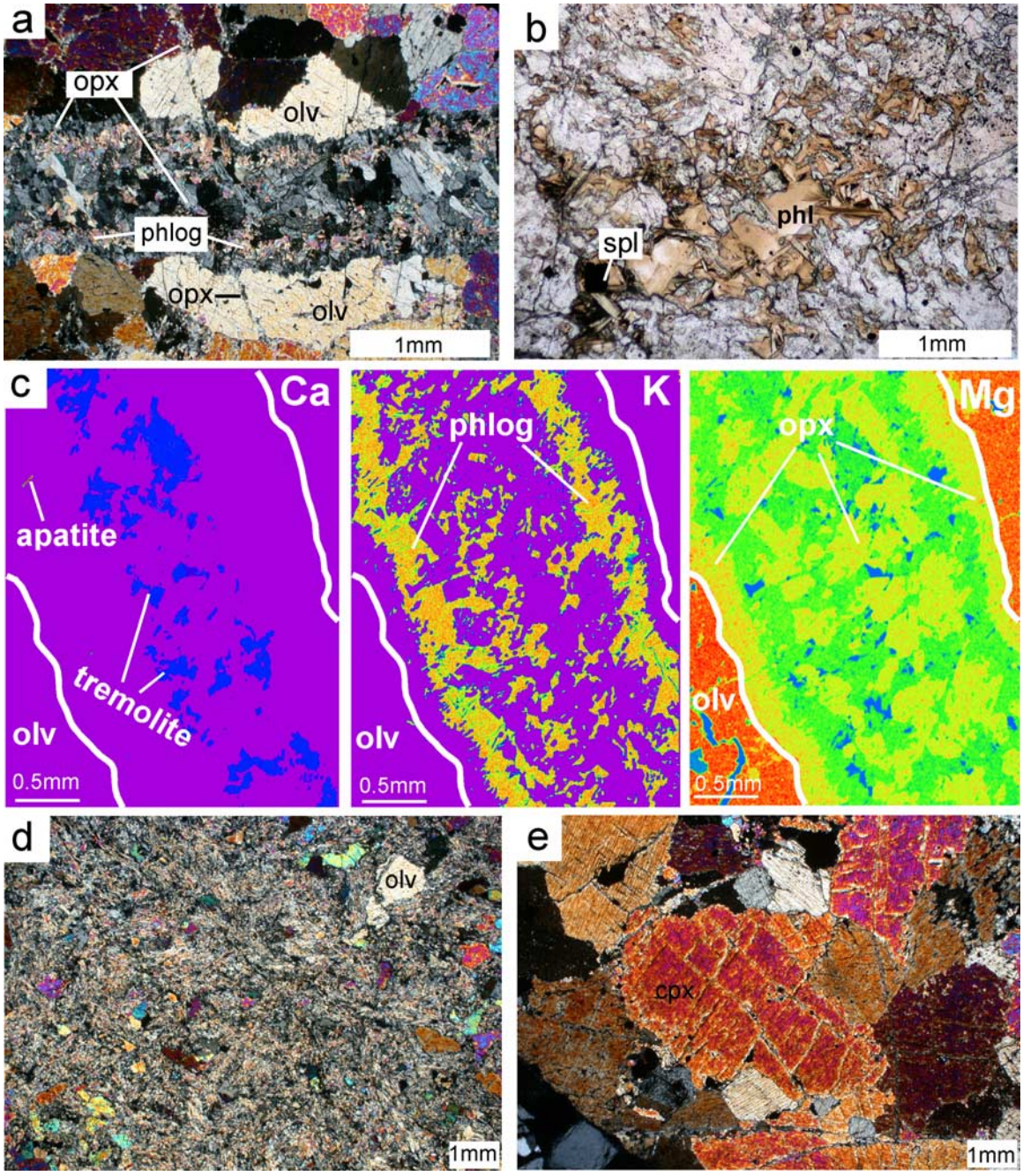

Figure 6. Photomicrographs and X-ray maps of Shiveluch xenoliths: (a) opx-amphibole-phlogopite vein crosscutting coarse-grained olivine and monomineralic veins of opx, (b) patch of phlogopite (brown) replacing spinel in lower left (black) in a harzburgite (plane-polarized light), (c) X-ray maps of calcium, potassium, and magnesium concentrations for the hydrous mineral vein from Figure 6a showing the distribution of opx, phlogopite, and amphibole, (d) hydrous phlogopite-bearing pyroxenite, and (e) coarse-grained clinopyroxenite xenolith.

and 5; Figure 9b). The correlation between Mg# in opx (100*Mg/Mg + Fe^{2+}) and Fo content in olivine in Figure 9a is similar to that observed in Mg-Fe^{2+} partitioning experiments between coexisting olivine and orthopyroxene at 1173 and 1273 K at 1.6 GPa [*von Seckendorff and O'Neill*, 1993]. In contrast, opx phenocrysts in the host melt are more Fe-rich than peridotite opx with an average Mg# = 72 (Table 5; Figure 9b). Exceptions to this narrow range in Mg#'s for opx in peridotites are those that

Table 2. Whole-Rock Major Element Compositions for Shiveluch Xenoliths Determined by XRF[a]

Sample	Rock Type	SiO_2	TiO_2	Al_2O_3	Cr_2O_3	FeO^t	MnO	MgO	NiO	CaO	Na_2O	K_2O	P_2O_5	Prenorm Total	LOI, %
SHX-03-01	harzburgite	47.44	0.06	1.27	0.29	6.30	0.14	43.92	0.22	0.32	0.22	0.30	0.03	99.99	−0.07
SHX-03-02	harzburgite	45.21	0.05	1.09	0.86	8.75	0.14	42.49	0.23	1.15	0.25	0.07	0.03	99.22	−0.44
SHX-03-03	harzburgite	45.01	0.01	0.56	0.82	7.64	0.14	44.98	0.27	1.07	0.14	0.05	0.02	99.62	−0.32
SHX-03-04	dunite	40.77	0.01	0.43	1.25	9.52	0.18	48.02	0.25	0.02	0.11	0.02	0.02	99.11	−0.56
SHX-03-07	lherzolite	45.09	0.08	1.09	0.68	8.82	0.15	40.95	0.26	2.92	0.22	0.09	0.02	99.43	−0.37
SHX-03-08	harzburgite	43.63	0.01	0.33	0.72	8.23	0.15	46.72	0.32	0.03	0.12	0.04	0.03	99.29	−0.40
SHX-03-10	lherzolite	42.35	0.05	0.89	0.93	11.32	0.25	42.60	0.28	1.50	0.21	0.04	0.02	99.23	−0.72
SHX-03-12	harzburgite	44.47	0.03	0.61	1.19	6.78	0.16	47.20	0.23	0.06	0.12	0.07	0.02	99.51	−0.24
SHX-03-17	harzburgite	42.36	0.01	0.76	1.56	8.19	0.19	47.01	0.22	0.11	0.13	0.19	0.03	98.97	−0.34
SHX-03-20	harzburgite	41.99	0.01	0.18	0.95	6.28	0.12	50.51	0.27	0.02	0.11	0.00	0.02	99.24	−0.22
SHX-03-21	lherzolite	46.17	0.09	1.44	0.59	9.59	0.17	37.67	0.07	5.04	0.17	0.02	0.03	100.39	−0.46
SHX-03-24	harzburgite	43.27	0.02	0.39	0.48	8.91	0.17	46.84	0.20	0.17	0.12	0.04	0.02	99.97	−0.49
SHX-03-26	harzburgite	42.92	0.03	0.50	1.22	7.54	0.10	47.81	0.23	0.06	0.11	0.04	0.03	99.13	−0.39
SHX-98-1	harzburgite	42.31	0.01	0.36	0.77	8.45	0.15	47.84	0.32	0.36	0.11	0.01	0.01	99.61	−0.65
SHX-98-16	harzburgite	42.68	0.07	1.77	0.86	9.95	0.24	42.92	0.19	1.48	0.29	0.29	0.03	99.72	−0.26
SHX-98-18	harzburgite	45.48	0.03	1.04	1.52	8.04	0.17	44.06	0.25	0.10	0.13	0.18	0.02	99.26	−0.23
SHX-98-2	harzburgite	43.62	0.02	0.35	0.96	6.89	0.12	48.06	0.25	0.04	0.10	0.02	0.03	99.25	0.72
SHX-98-5	harzburgite	42.10	0.03	0.85	1.10	7.71	0.15	47.82	0.19	0.19	0.18	0.15	0.03	99.22	−0.37
SHX-98-6	harzburgite	43.44	0.01	0.23	0.98	7.74	0.15	47.40	0.34	0.03	0.11	0.04	0.02	99.15	−0.47
SHX-98-7	harzburgite	42.99	0.02	0.72	0.92	9.46	0.19	44.75	0.29	0.84	0.16	0.07	0.03	99.23	−0.41
SHX-98-PT	harzburgite	43.82	0.02	0.60	0.45	7.21	0.20	48.69	0.21	0.05	0.11	0.03	0.03	100.77	−0.22
SHX-03-13	hydrous pyroxenite	51.83	0.03	0.78	0.60	6.40	0.12	33.14	0.23	7.05	0.22	0.03	0.02	99.61	−0.03
SHX-98-12	hydrous pyroxenite	54.39	0.03	1.03	1.06	7.13	0.15	32.37	0.17	4.41	0.24	0.04	0.03	99.81	−0.17
SHX-98-4	hydrous pyroxenite	49.74	0.09	1.86	0.99	8.98	0.17	36.47	0.20	1.59	0.24	0.41	0.05	99.60	0.08
SHX-03-19	clinopyroxenite	52.23	0.12	1.59	0.43	5.52	0.14	20.84	0.03	19.25	0.27	0.02	0.02	100.69	0.29
SHX-98-15	clinopyroxenite	52.19	0.15	2.06	0.41	6.04	0.15	19.30	0.05	19.67	0.35	0.08	0.02	99.99	0.02

[a] Anhydrous basis and normalized to a total of 100%. Whole-rock major element compositions are in wt%. Abbreviation: t, total iron expressed as FeO.

have crystallized near the edge of the xenoliths within 1–2 mm of the hornblende-host selvage, where Mg/Fe in olivine and opx are relatively low (Mg# ~ 80, Table 5).

[20] Clinopyroxene in the peridotite xenoliths is Cr-diopside (to 0.9 wt% Cr_2O_3) with Mg# (100*Mg/Mg + Fe^{2+}) from 94–98 (Table 3). The Mg# in cpx is positively correlated with the Mg# in opx and the Mg# in olivine for a given peridotite. Line scans across cpx grains coexisting with olivine and opx are homogeneous and show no significant change in MgO, FeO*, or CaO wt% from cores-to-rims (Figure 8).

[21] Amphibole within the peridotites is edenitic and tremolitic on the basis of thirty analyses in seven samples [*Leake et al.*, 1997], with Mg# from 86–92 and SiO_2 from 44.1–56.5 wt% (6.9–8.2 Si in formula; Figure 10). In contrast, amphiboles from the hornblende-host selvage, measured in two peridotite xenoliths, are pargasitic and similar to hornblende phenocrysts in the host andesite, with lower Mg# (66.2–77.8) and higher TiO_2 (0.92–1.1 wt%), FeO (10.1–12.7 wt%), and Al_2O_3 (11.7–12.2 wt%) compared to amphiboles from the interiors of the xenoliths (TiO_2 = 0.0–0.86 wt%; FeO = 2.8–6.3 wt%; Al_2O_3 = 1.4–10.2 wt%).

[22] Phlogopite Mg# ranges from 90–94 when it forms in veins and along spinel grain boundaries in the interior of the xenolith. In one harzburgite (SHX-98-16), phlogopite has crystallized next to the hornblende-host selvage and has a lower range of Mg# from 83–87 (Table 5). The Al_2O_3 and K_2O concentration in phlogopite covers a relatively narrow range from 14.6–16.9 wt% and 7.7–8.4 wt% and TiO_2 covers a wide range from 0.07–1.56 wt%.

5.2. Pyroxenites

[23] Mineral compositions for the hydrous pyroxenites are nearly identical to the peridotites, with Fo_{88-90} in olivine, Mg# from 95–98 in clinopyroxenes, Mg# from 90–94 in orthopyroxenes, Mg# from 90–94 in amphiboles, Mg# = 89 in phlogopites, and Cr# from 70–83 in spinels (Table 4;

Table 3. Representative EMP Analyses of Mineral Core Compositions in Shiveluch Peridotite Xenoliths[a]

Sample	SHX-03-04	SHX-03-08	SHX-03-07	SHX-03-04	SHX-98-06	SHX-03-07	SHX-03-04	SHX-98-01	SHX-03-10	SHX-98-07	SHX-03-07	SHX-03-17	SHX-03-17
Rock type Mineral	dunite olv	harzburgite olv	lherzolite olv	dunite opx	harzburgite opx	lherzolite opx	dunite spl	harzburgite spl	lherzolite spl	harzburgite cpx	lherzolite cpx	harzburgite amph	harzburgite phlog
SiO_2	41.12	40.00	39.54	56.16	57.40	56.53	0.02	0.07	0.07	54.51	54.39	53.39	41.72
TiO_2	0.01	0.01	0.00	0.02	0.00	0.08	0.53	0.13	0.26	0.07	0.06	0.04	0.08
Al_2O_3	0.00	0.00	0.00	1.85	0.54	1.36	15.58	11.26	9.84	1.04	0.74	5.15	14.94
Cr_2O_3	0.00	0.03	0.06	0.00	0.03	0.12	37.17	51.84	47.03	0.32	0.09	0.01	0.40
FeO*	9.14	8.33	11.17	6.27	5.49	7.26	33.53	25.64	32.48	2.98	2.91	3.76	4.22
MgO	50.36	51.27	48.91	35.19	36.14	34.79	11.01	10.18	8.46	19.25	17.96	22.34	24.92
CaO	0.02	0.03	0.01	0.39	0.19	0.40	0.00	0.00	0.00	21.30	23.69	11.91	0.05
NiO	0.20	0.27	0.40	0.01	0.07	0.09	0.17	0.13	0.11	0.04	0.05	0.17	0.12
Na_2O	0.00	0.07	0.00	0.06	0.11	0.00	0.03	0.06	0.00	0.32	0.19	1.14	0.97
K_2O	0.00	0.00	0.00	0.01	0.00	0.00	0.01	0.00	0.00	0.02	0.00	0.19	8.36
Total	100.85	100.02	100.12	99.96	99.99	100.62	98.06	99.32	98.25	99.86	100.09	98.09	95.78
Mg#	90.8	91.7	88.6	94.5	95.0	92.5	52.6	49.8	42.3	94.2	94.8	91.4	91.3
Cr#							61.5	75.5	76.2				
$Fe^{3+}/\Sigma Fe$				0.42	0.39	0.30	0.49	0.30	0.38	0.29	0.39		

[a] Mg#, 100*Mg/(Mg + Fe2+) for pyroxenes and spinel and 100*Mg/(Mg + total Fe) for olivine; Cr#, 100*Cr/(Cr + Al); $Fe^{3+}/\Sigma Fe$ values for spinels and pyroxenes were estimated assuming stoichiometry [*Droop*, 1987] and used to calculate pressure, temperature, and oxygen fugacity listed in Table 6.

Table 4. Representative EMP Analyses of Minerals in Shiveluch Pyroxenite Xenoliths[a]

Sample	SHX-03-19	SHX-03-13	SHX-03-19	SHX-03-13	SHX-98-15	SHX-98-12	SHX-03-19	SHX-98-15	SHX-98-12	SHX-03-13	SHX-98-04
Rock type	cp	hp	cp	hp	cp	hp	cp	cp	hp	hp	hp
Mineral	olv	olv	opx	opx	spl	spl	cpx	cpx	cpx	amph	phlog
SiO_2	39.22	40.57	55.90	57.57	0.01	0.05	53.59	54.68	54.54	56.54	40.53
TiO_2	0.04	0.03	0.02	0.01	1.01	0.32	0.13	0.03	0.04	0.05	0.63
Al_2O_3	0.00	0.00	0.88	0.37	3.00	8.74	1.24	0.32	0.32	1.39	14.73
Cr_2O_3	0.05	0.00	0.01	0.05	5.88	49.23	0.17	0.03	0.17	0.04	0.80
FeO*	16.86	9.69	10.21	6.54	78.54	32.15	4.20	2.15	2.63	2.88	5.17
MgO	44.55	49.37	31.88	35.08	6.53	8.12	17.28	17.97	18.71	23.40	24.26
CaO	0.06	0.04	0.75	0.40	0.00	0.01	23.09	24.76	23.56	12.32	0.11
NiO	0.18	0.34	0.07	0.22	0.29	0.24	0.07	0.08	0.26	0.14	0.20
Na_2O	0.04	0.02	0.05	0.02	0.00	0.05	0.31	0.03	0.05	0.43	0.87
K_2O	0.00	0.00	0.01	0.00	0.00	0.02	0.01	0.01	0.00	0.00	8.38
Total	101.03	100.06	99.79	100.27	95.26	98.93	100.09	100.06	100.28	97.20	95.69
Mg#	82.5	90.1	86.6	91.9	33.9	40.8	92.9	95.7	96.5	93.5	89.3
Cr#					56.8	79.1					
$Fe^{3+}/\Sigma Fe$			0.14	0.16	0.73	0.36	0.44	0.33	0.53		

[a] Abbreviations: hp, hydrous pyroxenite; cp, clinopyroxenite.

Table 5. Representative EMP Analyses of Minerals in Hornblende-Host Selvage, Andesite Host Rock, and Veins

Sample	SHX-98-16	SHX-98-02	SHX-98-15	SHX-03-17	SHX-03-17	SHX-98-16	SH98-64	SHX-98-18	SHX-03-12	SHX-98-16
Number[a]	1	2	3	4	5	6	7	8	9	10
Mineral	olv	opx	opx	opx	amph	amph	amph	phlog	phlog	phlog
SiO_2	38.87	55.60	54.09	57.41	54.21	42.12	44.77	42.28	42.80	38.61
TiO_2	0.03	0.01	0.05	0.01	0.00	1.07	2.16	0.21	0.92	0.40
Al_2O_3	0.00	0.65	0.44	0.85	4.54	12.18	9.63	15.35	14.67	16.30
Cr_2O_3	0.00	0.02	0.04	0.02	0.00	0.00	0.10	0.06	0.89	0.05
FeO*	11.03	13.25	18.11	7.70	3.48	12.74	12.71	3.62	2.81	7.69
MgO	49.79	30.29	26.31	34.79	22.53	13.99	14.40	25.44	25.36	21.81
CaO	0.03	0.39	0.87	0.24	11.62	11.26	11.18	0.07	0.09	0.07
NiO	0.39	0.05	0.01	0.04	0.18	0.00	0.00	0.36	0.17	0.11
Na_2O	0.01	0.03	0.02	0.09	1.02	2.13	2.06	1.19	1.38	1.03
K_2O	0.00	0.00	0.01	0.00	0.10	0.74	0.46	8.06	7.65	8.27
Total	100.18	100.28	99.95	101.15	97.67	96.23	97.47	96.65	96.74	94.33
Mg#	89.0	82.0	73.8	91.3	92.0	66.2	66.9	92.6	94.2	83.5
$Fe^{3+}/\Sigma Fe$		0.11	0.08	0.23						

[a] 1, olivine next to opx-amph-phlog vein; 2, orthopyroxene next to hornblende host selvage; 3, orthopyroxene phenocrysts in the andesite host rock; 4, orthopyroxene coexisting with amphibole and phlogopite in vein; 5, tremolitic amphibole coexisting with opx and phlog in vein; 6, amphibole phenocryst in hornblende-host selvage; 7, amphibole phenocryst in host rock; 8, phlogopite in patches that replace Cr-spinel; 9, phlogopite in vein; 10, phlogopite next to hornblende-host selvage.

Table 6. Equilibration Temperature, Pressure, and Oxygen Fugacity Calculated for Shiveluch Xenoliths[a]

Sample	$T°C_{(OW)}^{Olv\text{-}Spl}$	$T°C_{(B)}^{Olv\text{-}Spl}$	$T°C^{two\text{-}pyroxene}$	$T°C^{Ca\text{-}in\text{-}opx}$	P, GPa	fO_2 (B)	fO_2 (W)	$Fe^{3+}/\Sigma Fe$ Spinel	Cr# Spinel	Fo Olivine	Ca-in-olv, ppm
SHX-03-01	710	714							55.3	91.4	
SHX-03-02	794	763				1.95	1.98	0.36	82.5	89.4	
SHX-03-03	716	706	826	783	2.21	2.70	2.59	0.42	73.3	91.6	259
SHX-03-04	836	824				2.70	2.48	0.49	61.5	90.6	
SHX-03-07	860	828	920	875	1.66	2.89	1.73	0.52	58.8	86.7	309
SHX-03-08	756	740							82.1	91.3	
SHX-03-10	851	803	1013	1081	1.85	1.84	1.60	0.38	76.2	88.0	409
SHX-03-12	794	780							73.0	92.2	
SHX-03-17	843	820							71.5	91.5	
SHX-03-20	624	640							61.5	93.4	
SHX-03-21	840	835	920	912	1.16				66.9	93.4	230
SHX-03-24	789	774							67.9	90.0	
SHX-03-26	692	694							65.6	92.5	
SHX-98-01	795	766	900	1035	1.32	1.44	1.68	0.30	75.5	91.1	302
SHX-98-02	708	720							67.0	92.7	
SHX-98-05	842	821							77.3	91.6	
SHX-98-06	762	744				1.72	2.02	0.32	79.7	91.7	
SHX-98-07	819	773	796	1045	1.03	1.42	1.36	0.31	77.1	89.2	323
SHX-98-16	761	734	837	885	1.25	0.89	1.41	0.27	73.2	88.5	244
SHX-98-16v			829		1.18					88.8	238
SHX-98-18	679	675				1.77	2.30	0.31	73.1	92.3	
SHX-98-PT	713	717				1.01	1.79	0.27	63.9	92.8	
SHX-03-13	802	772				2.49	2.33	0.42	83.2	90.0	
SHX-98-04	833	793	894	808	1.32	1.79	1.67	0.38	80.9	87.6	300
SHX-98-12	759	743				2.70	2.34	0.47	80.2	88.9	
SHX-03-19	853	837				4.53	3.30	0.67	37.5	83.9	
SHX-98-15						4.10	2.43	0.73	56.8	83.7	

[a] Olivine-spinel temperatures are (OW) from *O'Neill and Wall* [1987] and (B) *Ballhaus et al.* [1991]. Two-pyroxene and Ca-in-opx temperatures are from *Brey and Köhler* [1990]. Pressure was calculated using the Ca-in-olivine barometer of *Köhler and Brey* [1990] using techniques described in the text. Oxygen fugacity estimates are from (B) *Ballhaus et al.* [1991] and (W) *Wood et al.* [1990] and are reported as Δlog fO_2 from the quartz-fayalite-magnetite (FMQ) buffer using the $Fe^{3+}/\Sigma Fe$ values of the spinels listed. SHX-98-16v are P-T estimates for the opx-amph-phog vein; olivine used in this calculation is located adjacent to the vein.

Figures 7 and 9). The clinopyroxenite compositions are generally more Fe-rich and plot off of the mantle array at lower forsterite contents and lower Mg# and Cr# in spinel (Figure 7), similar to cumulate-type ultramafic rocks from the Great Dyke in Zimbabwe [*Wilson*, 1982], Kharchinsky Volcano, Kamchatka [*Dektor et al.*, 2005], and from some Aleutian xenoliths [*DeBari et al.*, 1987].

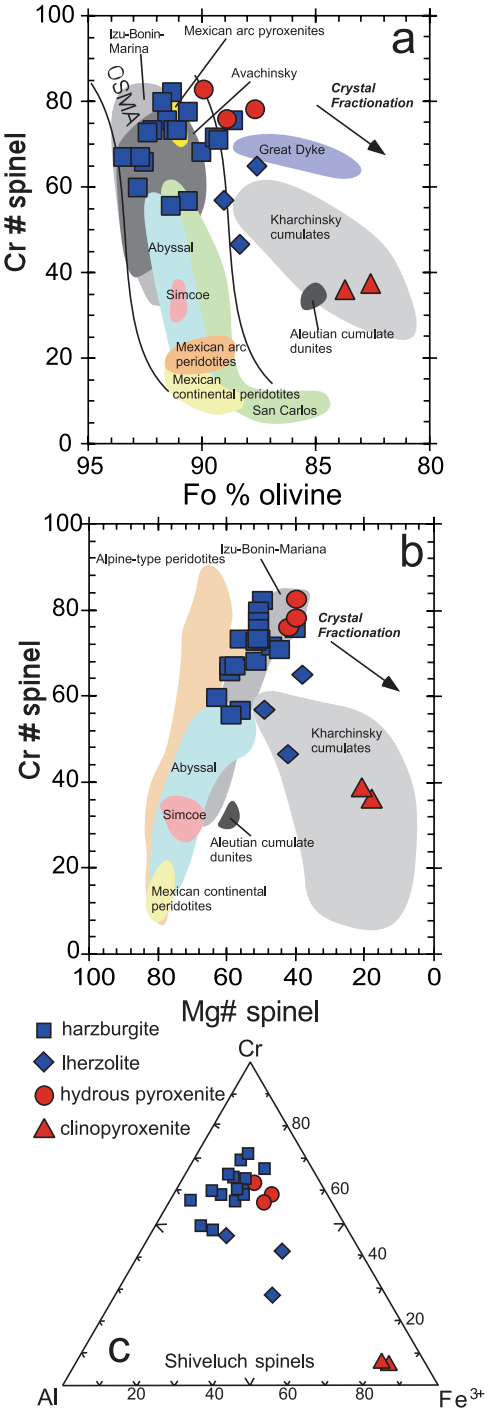

6. Discussion

6.1. Physical Conditions of Xenolith Equilibration (P-T-fO_2)

[24] Mineral compositions described above imply that the xenoliths, including the hydrous mineral veins that crosscut the peridotites, are in general, well equilibrated (Figure 8), and are therefore appropriate for estimating temperature, pressure, and oxygen fugacity. In contrast, minerals that have crystallized on the margins of the xenoliths, adjacent to the hornblende-host selvage, and phenocrysts within the andesite host melt show significant compositional zoning and are compositionally distinct from those that form in the veins and in the interior of the xenoliths (Figures 9c and 10; Tables 3 and 5). This indicates that the P-T-fO_2 conditions recorded in the xenoliths are probably unaffected by the formation of the hornblende-host selvage, which we interpret as being produced at shallow depths in the magma chamber by reactions between the hydrous andesitic host melt and olivine in the xenoliths during transport to the surface.

[25] Equilibration pressures were calculated using the Ca-exchange barometer between coexisting olivine and cpx from *Köhler and Brey* [1990]. This barometer was calibrated specifically for spinel

Figure 7. Average olivine and spinel core compositions for Shiveluch xenoliths. The Fo% for olivine is 100*Mg/(Mg + Fe), Cr # for spinel is 100*Cr/(Cr + Al), and Mg # for spinel is 100*Mg/(Mg + Fe^{2+}). The Fe^{3+} for spinel (Figure 7c) was estimated assuming stoichiometry [*Droop*, 1987]. The Olivine-Spinel Mantle Array (OSMA) is from *Arai* [1994], and the crystal fractionation trends are from *Dick and Bullen* [1984]. Also shown are spinel-olivine compositions for ultramafic rocks from the Izu-Bonin-Mariana [*Parkinson and Pearce*, 1998], Avachinsky, Kamchatka [*Arai et al.*, 2003], Simcoe, WA [*Brandon and Draper*, 1996], Mexican continental peridotites [*Luhr and Aranda-Gomez*, 1997], Mexican arc peridotites and websterites [*Blatter and Carmichael*, 1998], San Carlos [*Frey and Prinz*, 1978], the Aleutians [*DeBari et al.*, 1987], Kharchinsky, Kamchatka [*Dektor et al.*, 2005], Great Dyke in Zimbabwe [*Wilson*, 1982], and Alpine-type and Abyssal peridotites [*Dick and Bullen*, 1984]. The Fo contents of olivine in the two clinopyroxenites have not been corrected for low-temperature Fe-Mg exchange between olivine and cpx [e.g., *Obata et al.*, 1974].

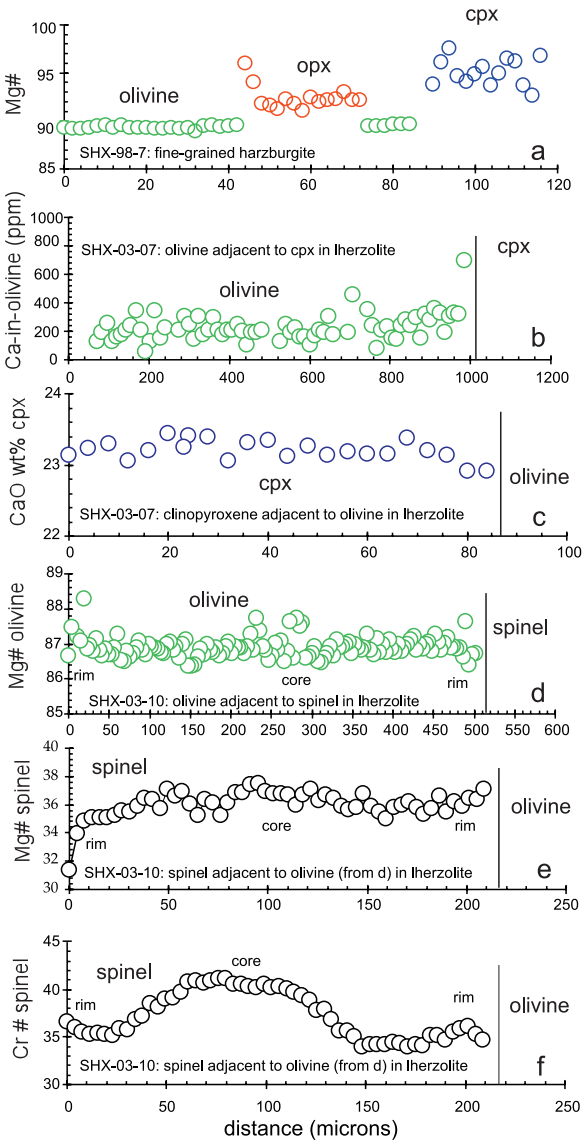

Figure 8. Line scans across mineral grains in Shiveluch xenoliths. Minerals present in each traverse are shown in the figure. The Mg# for pyroxenes and spinel is 100*Mg/(Mg + Fe^{2+}) and 100*Mg/(Mg + Fe) for olivines. The compositional homogeneity in these coexisting minerals suggests that the xenoliths are well-equilibrated and are therefore appropriate for estimating temperature and pressure using two-pyroxene and olivine-spinel thermometry and Ca-in-olivine barometry. The occasional variation in Mg#-Cr# in spinel (Figures 8e and 8f) is over a narrow range and affects the olivine-spinel temperatures calculated from these data by <5°C. Note that the spinel in Figures 8e and 8f coexists with the olivine in Figure 8d.

peridotites with experiments from 0.2–6.0 GPa and 900–1400°C (Table 6). Many of the Shiveluch xenoliths, especially the abundant harzburgites, lack well-developed cpx-olivine mineral assemblages, and because of this we were able to obtain pressures for only four harzburgites, three lherzolites, and one hydrous pyroxenite. The pressures calculated for these eight spinel-bearing xenoliths range from 1.03–2.21 GPa (Table 6; Figure 11).

[26] The Ca-in-olivine exchange barometer is extremely sensitive to temperature, such that a difference of 100°C used in the barometer will produce a calculated pressure difference of 1.2 GPa. Because of this, we have used a nominal pressure of 1.5 GPa and the two-pyroxene thermometer of *Brey and Köhler* [1990] to calculate a nominal, pressure-standardized temperature, which in turn was used to calculate the pressure recorded in the rocks by the Ca-in-olivine exchange barometer. We do this because the two-pyroxene thermometer is essentially independent of pressure (a 1.0 GPa shift in pressure for this thermometer changes the calculated temperature by only 17°C), so the use of a 1.5 GPa-normalized temperature from this thermometer removes the very large amount of variability in the Ca-in-olivine pressures which would otherwise be introduced by temperatures which are themselves uncertain by several tens of degrees. This approach is also justified because the xenoliths are dominated by one or two rock types, with similar textural and compositional features, indicating that most of the samples probably equilibrated under similar P-T conditions beneath Kamchatka.

[27] *Köhler and Brey* [1990] showed that their calibration reproduces experimental conditions to within ±0.54 GPa when combined with the two-pyroxene thermometer. We have taken this ±0.54 GPa as our error on pressure for all xenoliths because the error in our microprobe measurement of Ca-in olivine is relatively small, and because all pressures were calculated with (1.5 GPa-normalized) temperatures from the two-pyroxene thermometer, which was reproduced on natural peridotites to within ±16°C [*Brey and Köhler*, 1990]. Despite the relatively large error in estimating pressure in this way, the pressures recorded in the Shiveluch xenoliths fall entirely within the experimentally determined stability field for spinel lherzolite (Figure 11).

[28] Temperature estimates were made using the Ca-in-opx and two-pyroxene Fe-Mg exchange thermometers of *Brey and Köhler* [1990] and the olivine-spinel Fe-Mg exchange thermometers of *Ballhaus et al.* [1991] and *O'Neill and Wall* [1987]. All temperatures reported in Table 6 were calculated using 1.5 GPa as the pressure term (as

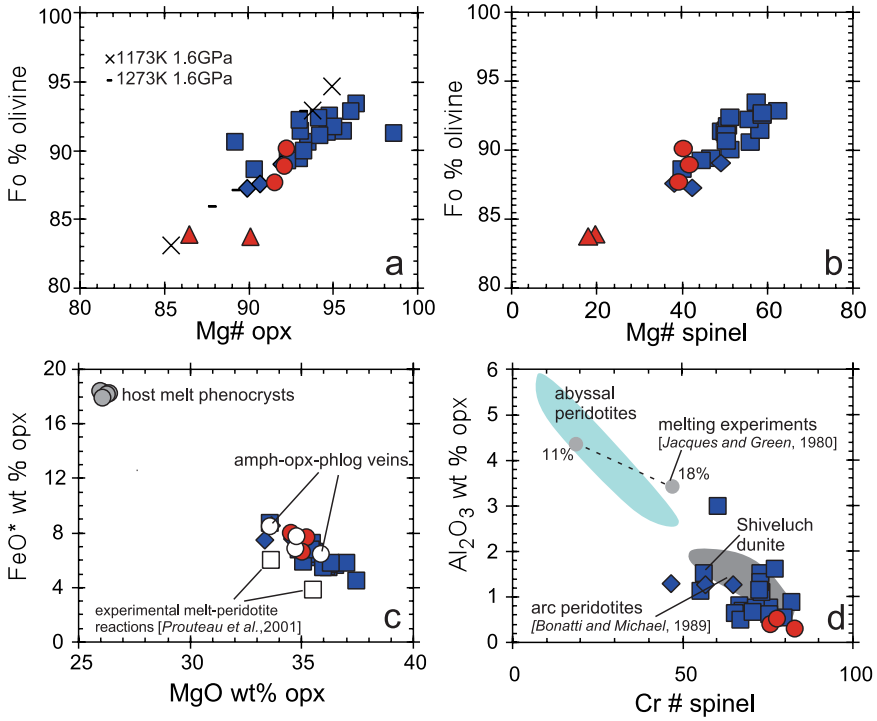

Figure 9. Coexisting orthopyroxene (opx), olivine, and spinel core compositions for Shiveluch xenoliths compared to phenocryst compositions in the host andesite. Symbols for Shiveluch xenoliths in this figure are as in Figure 3. Figures 9a and 9b show olivine forsterite content (Fo%) compared to Mg# (100*Mg/Mg + Fe^{2+}) in coexisting opx and Mg# (100*Mg/Mg + Fe^{2+}) in spinel. Also shown in Figure 9a are equilibrium experimental results at 1173 K and 1273 K at 1.6 GPa for coexisting opx and olivine from *von Seckendorff and O'Neill* [1993]. Olivine, opx, and spinel are average mineral core compositions. Figure 9c shows the total FeO (FeO*) and MgO in opx in Shiveluch xenoliths compared to phenocryst compositions from the host andesite. Orthopyroxene compositions for xenoliths are average mineral core compositions. Orthopyroxene compositions from experimentally produced melt-peridotite reactions are from *Prouteau et al.* [2001]. These experiments involved the reaction of a trondjhemite melt with mantle-like olivine (Fo_{90}) at 900–1000°C and 15 kb under hydrous conditions (7.8–9.6 wt% H_2O). Host melt opx phenocrysts are from five different analyses in one sample. Figure 9d shows Al_2O_3 in opx plotted against Cr# (100*Cr/Cr + Al) in coexisting spinel for Shiveluch peridotite and pyroxenite. Abyssal (North Atlantic) and subduction margin (Tonga and Mariana) peridotite fields are from *Bonatti and Michael* [1989]. The dashed line indicates the experimental compositions of *Jaques and Green* [1980] for residual peridotites from 11% and 18% melting of a Tinaquillo peridotite.

described above) instead of the calculated Ca-in-olivine pressure for consistency with other published temperature estimates [e.g., *Parkinson and Pearce*, 1998]. The two-pyroxene Fe-Mg exchange and Ca-in-opx thermometers require coexisting cpx and opx and, as discussed above, can only be applied to xenoliths that have well-developed pyroxene pairs and homogeneous core to rim compositions that demonstrate equilibration (Figure 8). The nine xenoliths that fit the criteria for two-pyroxene and Ca-in-opx thermometry record temperatures that are in general agreement with a range from 783–1081°C (Table 6). Our best estimate for the temperature and pressure in the opx-amphibole-phlogopite veins is 829°C and 1.18 GPa, based on opx within a vein in a harzburgite xenolith (SHX-98-16) and coexisting olivine and cpx adjacent to the vein (Figure 11). The P-T conditions calculated in this way are also consistent with the presence of tremolitic amphibole, which we observe in three of our samples (SHX-98-16, SHX-03-17, SHX-03-13), and based on the experimentally determined stability fields for tremolite from *Chernosky et al.* [1998] and *Jenkins* [1983].

[29] The olivine-spinel Fe-Mg exchange thermometers of *Ballhaus et al.* [1991] and *O'Neill and Wall* [1987] were applied to all of the studied xenoliths because olivine and spinel coexist in all samples. These calibrations produce the same temperature (R^2 = 0.95) with a range from 624–860°C

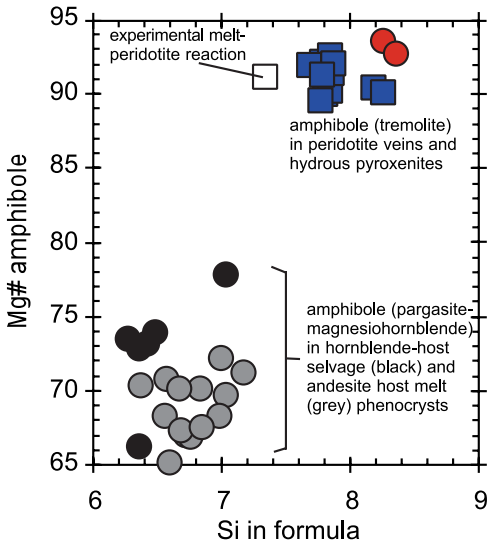

Figure 10. Representative amphibole core compositions for Shiveluch xenoliths, hornblende-host selvage, and andesite host melt phenocrysts. Amphibole in harzburgites and hydrous pyroxenites is edenitic and tremolitic [*Leake et al.*, 1997] and occurs in veins with opx and phlogopite, inclusions within spinel, and along cpx grain boundaries. Amphiboles from the hornblende-host selvage and phenocrysts in the host andesite are classified as pargasite and magnesiohornblende. Data source for experimental melt-peridotite reactions is the same as in Figure 9. Symbols for Shiveluch xenoliths are as in Figure 3 or are identified in the figure.

(Table 6). Two-pyroxene temperatures from Shiveluch xenoliths are consistently higher than olivine-spinel temperatures by an average of 89°C. This observation may be due to the higher diffusion rates of Fe and Mg in olivine and spinel compared to pyroxenes, which could produce lower olivine-spinel temperatures if the xenoliths were recording a cooling history [*Franz et al.*, 2002].

[30] *Ozawa* [1983] showed that systematic variations in spinel grain size and Mg# from core to rim in spinel and olivine in peridotites from Japan, caused by heating and cooling events, can result in two hundred degree differences in the calculated olivine-spinel temperatures. To investigate the origins of the olivine-spinel temperatures in our samples, we have done multiple line scans across coexisting olivine and spinel pairs for peridotites that cover the entire range of calculated temperatures and for spinel grains coexisting with olivine that vary in size from 85 μm to 900 μm. We find that Mg and Fe^{2+} in spinel and olivine in the Shiveluch xenoliths varies over a narrow range from core to rim, regardless of spinel grain size, and these variations have little effect on calculated temperatures (Figures 8d and 8e). For example, the variation in Fo content in olivine and Mg#-Cr# in the coexisting spinel grain in Figures 8d, 8e, and 8f correspond to a variation in temperature of only 5°C from core to rim. We have also analyzed 106 points on a 900 μm spinel grain from the same xenolith and found that the Mg# is nearly identical (Mg# $\approx$ 37) to the 200 μm spinel from the line scan in Figure 8, and therefore produces a similar temperature. This is in contrast to the significant variations in Fo% in olivine (up to 4%) and Mg# in spinel (up to 10) observed by *Ozawa* [1983] for the Japan peridotites over a similar range of spinel grain size. These observations, including the strong correlation between average core compositions of Fo% in olivine and Mg# in spinel (Figure 9b), indicate that the temperatures that we have calculated using the spinel and olivine core compositions are probably good estimates of the equilibration temperatures and are not strongly affected by ther-

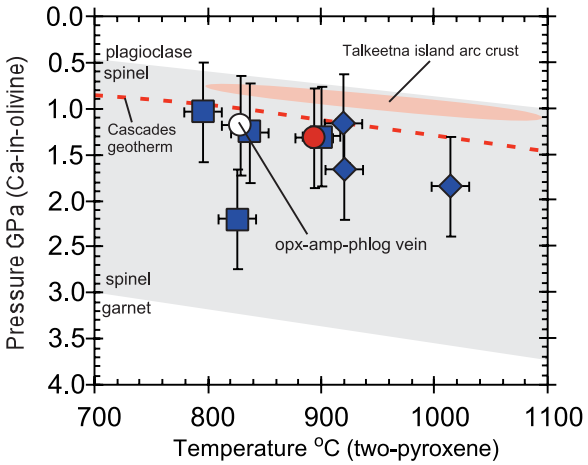

Figure 11. Equilibration P-T estimates for Shiveluch xenoliths using two-pyroxene thermometry [*Brey and Köhler*, 1990] and Ca-in-olivine barometry [*Köhler and Brey*, 1990]. Analytical techniques and errors are described in the text. The Fe^{2+} component, which was estimated assuming pyroxene stoichiometry [*Droop*, 1987], was used in the two-pyroxene temperature calculations. The plagioclase-spinel-garnet stability field is from *Herzberg* [1978] and *O'Neill* [1981]. The spinel-garnet transition is calculated for spinel with Cr# = 0.72, which is the average of the eight xenoliths reported in Table 5. Cascades geotherm is from the thermal model of *van Keken et al.* [2002], based on a crustal density of 2.6 g/cm^3. Talkeetna arc crust is based on P-T estimates for garnet gabbros and gabbronorites from *Kelemen et al.* [2003] and *DeBari and Coleman* [1989]. Symbols for Shiveluch xenoliths are as in Figure 3.

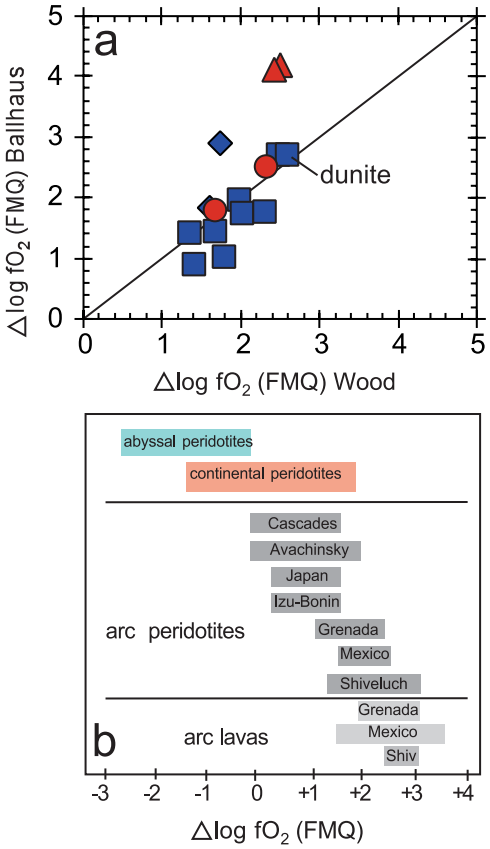

Figure 12. Oxygen fugacity calculated for Shiveluch xenoliths compared to published data for peridotites and arc lavas. Estimates of fO_2 plotted in Figure 12a were made using the methods of *Ballhaus et al.* [1991] and *Wood et al.* [1990] and are plotted as log fO_2 units from the fayalite-magnetite-quartz buffer reaction. Symbols for Shiveluch xenoliths are as in Figure 3. Figure 12b shows the total range of fO_2 calculated from the Shiveluch xenoliths (bottom gray bar under "arc peridotites") compared to published data from other peridotites and from arc lavas. Oxygen fugacities for other data sources are as follows: abyssal [*Bryndzia and Wood*, 1990], continental [*Wood and Virgo*, 1989], Cascades [*Brandon and Draper*, 1996], Avachinsky Volcano, Kamchatka [*Arai et al.*, 2003], Japan [*Wood and Virgo*, 1989], Izu-Bonin-Mariana [*Parkinson and Pearce*, 1998], Grenada [*Parkinson et al.*, 2003], Mexican hornblende-bearing peridotites and websterites [*Blatter and Carmichael*, 1998], Mexican hornblende andesites [*Carmichael*, 1991], and Shiveluch (Shiv) andesites [*Humphreys et al.*, 2006].

mal events, which result in incomplete equilibration of the mineral pairs.

[31] On the basis of two-pyroxene thermometry and Ca-in-olivine barometry, the P-T conditions of the xenoliths range from 1.03–2.21 GPa and 796–1013°C (Figure 11; Table 6). This suggests that the last equilibration of the xenoliths was just below the Moho at a depth of approximately 35–45 km and supports geophysical estimates which have shown that the crust beneath Shiveluch is approximately 30–35 km thick [*Levin et al.*, 2002]. Our results also suggest that the P-T conditions of the Moho beneath Shiveluch Volcano are similar to those in the Cascades, based on the model of *van Keken et al.* [2002], but slightly cooler at a given depth than the Talkeetna island arc [*DeBari and Coleman*, 1989; *Kelemen et al.*, 2003].

[32] Oxygen fugacity estimates have been calculated using the methods of *Ballhaus et al.* [1991] and *Wood et al.* [1990] according to the well-calibrated heterogeneous equilibrium among coexisting olivine, spinel, and opx. These results are reported in Table 6 as fO_2 log units from the fayalite-magnetite-quartz oxygen buffer or FMQ. These oxygen barometers produce fO_2 estimates that are similar at relatively low fO_2 values (r^2 = 0.76 in harzburgites), but can vary by as much as 1.7 ΔFMQ in the most oxidized samples, such as the clinopyroxenites (Table 6; Figure 12). Overall, the Shiveluch xenoliths are among the most oxidized of any xenolith suite reported, with fO_2 in peridotites from +1.3 to +2.6 ΔFMQ, hydrous pyroxenites from +1.6 to +2.5 ΔFMQ, and clinopyroxenites from +2.4 to +3.3 ΔFMQ using the *Wood et al.* [1990] calibration (Table 6). This range of high fO_2 for the Shiveluch xenoliths is similar to those seen in hornblende-bearing peridotite and pyroxenite xenoliths from central Mexico [*Blatter and Carmichael*, 1998] and for recently reported fO_2 values for arc lavas from Shiveluch [*Humphreys et al.*, 2006].

6.2. Origin of Dunite Protolith

[33] Perhaps the most interesting feature of these xenoliths is that opx, which can be present from 7–45 wt% in peridotites and to 72 wt% in hydrous pyroxenites, is always fine-grained and fibrous and recognized as a secondary or late-stage mineral phase present only along olivine grain boundaries, in monomineralic veins that crosscut coarse olivine grains, and in veins with amphibole and phlogopite (Figures 4, 5, and 6). This fibrous form of opx in the Shiveluch xenoliths contrasts the nature of opx in other xenoliths from Kamchatka and elsewhere [e.g., *Arai et al.*, 2003], where opx in harzburgites is commonly coarse and blocky and texturally similar to the associated olivine. These textural

relationships are important because they imply that the harzburgite, lherzolite, and hydrous pyroxenites from Shiveluch were probably all originally dunites. If this is true, it implies that orthopyroxene, phlogopite, and amphibole in the xenoliths were added primarily by processes subsequent to dunite formation.

[34] The genesis of dunite in arc-settings is generally viewed in the context of (1) cumulates formed by crystal fractionation from an olivine-rich, picritic magma [*DeBari et al.*, 1987], (2) residues of very high degrees of depletion involving multiple melt extraction events in the presence of water [*Bonatti and Michael*, 1989; *Dick and Bullen*, 1984], and (3) melt-rock reactions which dissolve pyroxene and precipitate olivine in the upper mantle [*Kelemen*, 1990; *Kelemen et al.*, 1995a]. The plausibility of these scenarios for the formation of the original dunite mineralogy of the Shiveluch peridotites is discussed below.

[35] The forsterite content in olivine, Cr# and Mg# in spinel, modal abundance of olivine, and Al_2O_3 in orthopyroxene have been shown to be sensitive indicators of the crystallization and melting histories of peridotites [*Arai*, 1994; *Bonatti and Michael*, 1989; *Boyd*, 1989; *Dick and Bullen*, 1984; *Dick and Fisher*, 1984; *Dick et al.*, 1984; *Jaques and Green*, 1980]. Partial melting will drive residual peridotites toward high forsterite in olivine, high Cr# in spinel, low Al_2O_3 in orthopyroxene, and high modal olivine. In contrast, crystal fractionation over a wide range of temperatures and melt Mg# will drive compositions in cumulate peridotites toward low forsterite and low Mg#-Cr# in spinel [*Dick and Bullen*, 1984]. On these criteria, the Shiveluch peridotites are refractory mantle samples (Fo_{88-94} olivine and Cr# = 47–82, Mg# = 38–69 in spinel, Al_2O_3 <2 wt% in opx) that fall within the olivine-spinel mantle array (OSMA) (Figure 7a) of *Arai* [1994] and the partial melting/residual mantle trends of *Dick and Bullen* [1984]. This relatively narrow and high range of forsteritic olivine and high Mg#-Cr# spinel in the Shiveluch xenoliths clearly contrast the trends of Fe-enrichment produced during olivine fractionation and observed in nearly all cumulates recognized in ultramafic complexes and in xenoliths [*Arai*, 1994; *DeBari et al.*, 1987; *Dick and Bullen*, 1984; *Greene et al.*, 2006; *Ozawa*, 1994; *Wilson*, 1982, Figure 7]. Comparison with xenoliths from other nearby areas in Kamchatka, also support a non-cumulate origin for the dunite protoliths at Shiveluch. Specifically, our collection of more than 250 xenoliths from Kharchinsky volcano, which is located 20 km to the southwest of Shiveluch, is dominated by pyroxenite and olivine pyroxenite which show highly variable Mg# in pyroxene, olivine and spinel, consistent with a cumulate origin [*Dektor*, 2006]. Mineral compositions in the cpx-rich xenoliths from Kharchinsky resemble those in the Shiveluch clinopyroxenites, based on their Fe-rich olivine (Fo_{83-84}) and spinel compositions which plot to the right in Figure 7. On the basis of these criteria, we interpret the clinopyroxenite xenoliths from Shiveluch as cumulates, but rule out a likely origin for the dunite protoliths to the Shiveluch peridotites through cumulate processes.

[36] Experimental studies also appear to rule out an origin for the Shiveluch dunite protoliths by melt extraction and depletion. In particular, experiments by *Jaques and Green* [1980] showed that residual dunites formed by ~50% melting would have Fo_{95} olivine and Cr# spinel ~80, a compositional range not observed in any peridotite that we have sampled. Specifically, the most depleted and least metasomatized Shiveluch peridotite, based on whole rock composition and modal mineralogy (dunite sample SHX-03-04, 90% olivine, MgO = 48%; Tables 1 and 2), has a spinel Cr# of 62 and olivine compositions of Fo_{91}. Again, these features are inconsistent with the experimentally determined mineral compositions produced in peridotite by melt extraction [*Jaques and Green*, 1980].

[37] Having ruled out cumulate and residual mantle origins, we now turn to the melt-rock reaction, which appears to be the most likely origin for the Shiveluch dunite protoliths, based on their overall mineral compositions. The process of melt-rock-reaction and its relationship to dunite formation was investigated by *Kelemen* [1990] and *Kelemen et al.* [1990], who showed through theoretical and experimental treatments that reactions between basaltic magma and peridotite can produce refractory dunite with uniformly forsteritic olivine compositions. This work is well supported by a variety of studies which have demonstrated that mafic melts move through porous networks of partially melted peridotite in the mantle [*McKenzie*, 1985; *Toramaru and Fujii*, 1986; *von Bargen and Waff*, 1986] and produce, at relatively low pressures, dunite channels by dissolution of pyroxene and crystallization of olivine [*Kelemen et al.*, 1995a, 1995b]. The importance of this process in the

control of melt flow through the mantle is supported by fluid dynamic modeling [*Aharonov et al.*, 1997] and by the widespread observation of discordant dunite in ophiolites [*Kelemen and Dick*, 1995; *Quick*, 1981].

[38] The Shiveluch xenoliths have the uniformly forsteritic olivine and Cr-rich spinel compositions predicted by the melt-rock-reaction process [*Dick and Bullen*, 1984; *Kelemen*, 1990, Figure 7a]. A melt-rock reaction origin for the dunite protolith is also consistent with the high fO_2 recorded in the Shiveluch peridotites (Figure 12). This point is discussed in detail below in section 6.3.

6.3. Origin of High fO_2

[39] The high oxygen fugacity recorded in the Shiveluch peridotites (fO_2 from +1.3–2.6 Δlog FMQ) compared to peridotites from abyssal, continental, and other arc-settings provide evidence that the xenoliths have retained a substantial amount of ferric iron as they evolved (Figure 12). *Brandon and Draper* [1996] argued that the fO_2 of peridotites from the Cascades could be explained by a two-step process involving the loss of ferric iron during melt extraction (due to the slightly higher incompatibility of Fe^{3+}) followed by later enrichment in ferric iron, and thus high fO_2, by oxidizing agents derived from subducted material. At Shiveluch, the sample that appears to be the least affected by metasomatic overprints (dunite sample SHX-03-04, 90% olivine, MgO = 48%; Tables 1 and 2) is nearly the most oxidized peridotite that we have analyzed, with fO_2 = +2.5 log units from FMQ (Figure 12a; Table 6). This depleted sample with high fO_2 indicates that oxidation of the Shiveluch xenoliths is not controlled by either melt extraction, which should produce low fO_2, or metasomatic enrichment, which should increase fO_2 [*Brandon and Draper*, 1996]. Oxygen fugacity in Shiveluch peridotites also appears to be uncorrelated with measures of depletion, such as Cr# in spinel, Fo in olivine, modal abundance of olivine, or whole-rock MgO. We also see little correlation between fO_2 and measures of geochemical enrichment, such as K, Ba or Rb concentrations, or with the presence of hydrous, metasomatic minerals such as phlogopite and/or amphibole.

[40] On the basis of the above, we conclude that oxidation state of the Shiveluch peridotites is not controlled in any clear way by either depletion or enrichment processes that may have affected the xenoliths. This implies that high fO_2 is a primary feature of the Shiveluch xenoliths, and that it was therefore probably acquired during the formation of the dunite protolith, prior to the formation of the hydrous mineral-bearing veins. If, as we have argued, the dunite protolith was produced by melt-rock interaction, then the oxidized nature of the peridotites reflects the oxidized nature of the subduction-derived melts that were involved in the melt-rock reaction process. This conclusion is well supported by the findings of *Parkinson and Arculus* [1999] and others [e.g., *Mungall*, 2002; *Parkinson and Pearce*, 1998] who have argued that melts are efficient oxidizers, and that the migration of melts through the mantle wedge provides a likely explanation for the high fO_2 which is widely observed in arc peridotites (Figure 12).

6.4. Deserpentinization or Metasomatism?

[41] Orthopyroxene in the Shiveluch peridotites is fibrous and radiating and forms primarily as thin coatings along olivine grain boundaries and in veins with amphibole and phlogopite that crosscut olivine and spinel (Figures 4, 5, and 6). The textural and compositional similarity of opx in the hydrous veins and along olivine grain boundaries seems to imply a common source and/or process (Figure 9c; Tables 3 and 5). It is an important point in this context that fibrous opx has been observed in certain alpine and arc-related peridotites, where it has been interpreted to result from dehydration reactions involving serpentine breakdown [*Arai and Kida*, 2000; *Trommsdorff et al.*, 1998]. It is therefore possible that the Shiveluch xenoliths are fragments of partially serpentinized peridotite that underwent prograde metamorphic reactions including deserpentinization. If this were true it would imply that the Shiveluch xenoliths are fragments of accreted oceanic lithosphere, and not samples of the sub-arc mantle.

[42] An important aspect of the fibrous opx in the Shiveluch xenoliths is that it commonly forms monomineralic coatings that outline in detail, 120° triple junctions among coarse olivine crystals (Figure 5). It is easy to imagine antigorite serpentine and related low-grade metamorphic minerals such as chlorite, similarly filling grain boundaries and fractures in a partially serpentinized peridotite; however, the prograde metamorphic transition from serpentine antigorite to olivine-enstatite rock produces not just fibrous enstatite, but also a variety of other minerals, such as chlorite, chro-

mian magnetite, pleochroic olivine, and talc, which are not observed in the Shiveluch peridotites [*Trommsdorff et al.*, 1998]. The presence of K-rich phlogopite in the veins, also cannot have resulted from the breakdown of serpentine alone, but is an expected feature of peridotites that have been metasomatized by subduction-related fluids or melts [e.g., *Franz et al.*, 2002; *Ionov et al.*, 1994]. The mineral chlorite, which is commonly present in serpentinized peridotites, and which is sustained during serpentine breakdown, is also not present in the Shiveluch xenoliths, even though it is stable under the P-T conditions that we calculate for many of our samples (e.g., 800–900 degrees C at 10–15 kb [*Goto and Tatsumi*, 1990; *Pawley*, 2003; *Smith and Riter*, 1997]). It is possible that the xenoliths were subjected to temperatures above chlorite stability and below the mantle solidus (e.g., 900–1100°C) which are not recorded in our temperature estimates. This possibility, however, fails to explain the presence of tremolite in the hydrous veins, which is stable only at temperatures below the chlorite stability field at pressures above 1 GPa [*Chernosky et al.*, 1998; *Jenkins*, 1983; *Smith and Riter*, 1997]. These and other textural and compositional features that have been interpreted to result from hydrous mineral breakdown in ultramafic xenoliths [e.g., *Smith and Riter*, 1997] indicate to us that the Shiveluch xenoliths have probably not experienced a history of serpentinization, and that they are therefore probably not pieces of accreted oceanic terranes [*Konstantinovakaia*, 2000] or partially subducted slices of such terranes.

6.5. Origin of Orthopyroxene, Amphibole, and Phlogopite

[43] Textural observations indicate that the Shiveluch xenoliths have experienced at least two observable stages of mineralization that post-date formation of the dunite protolith. These involve (1) the formation of opx along olivine grain boundaries and in monomineralic veins that crosscut coarse olivine (Figures 4f and 5) and (2) the final-stage formation of mm-scale veins of amphibole-phlogopite-opx (Figure 6a).

[44] An important first-order conclusion is that the distinct compositional differences between minerals in the veins and in the hornblende-host selvage areas indicate that the metasomatism/mineralization that we observe was not produced by the infiltration of the host melt into the xenoliths (Figures 9c and 10). The distinctive texture and mineralogy of the veins (containing fibrous opx, tremolite, phlogopite) and the absence of those features from the hornblende-host selvage areas also indicate that the veins and grain-boundary crystallization of secondary minerals within the xenoliths is unrelated to xenolith-host melt interaction.

[45] Textural and compositional similarities (Figures 4f, 5, and 9c) indicate that fibrous opx along grain-boundaries and in monomineralic veins were produced contemporaneously and by similar processes. The jagged and interpenetrating contacts (Figure 4f) indicate that the fibrous opx formed by replacement processes involving reactions between silica-rich fluids/melts and olivine. The absence of textural equilibrium between olivine and opx (indicated by jagged and interpenetrating contacts; Figure 4f) implies that the fibrous opx formed shortly prior to the eruption that carried the xenoliths to the surface. This probably means in turn that the silica-rich fluids/melts were liberated from hydrous magmas trapped in the uppermost mantle beneath Shiveluch.

[46] The textural and compositional similarity of fibrous opx throughout the rocks indicates that phlogopite-amphibole-opx veins, which are the final stage of mineralization recorded in the xenoliths (Figure 6a), were probably also formed by hydrous magmas that were trapped at shallow mantle levels. In particular, we interpret the hydrous veins as the products of volatile-enriched, deuteric/autometasomatic fluids/melts that were released during the final stages of magma crystallization in the uppermost mantle. Consistent with this interpretation, the vein mineral compositions in the xenoliths are similar to those observed in experimentally produced melt-peridotite reactions [*Prouteau et al.*, 2001]. It is interesting to speculate that the Shiveluch xenoliths might illustrate a continuum of melt-rock reaction products and relationships, which began with the creation of the dunite protolith and ended with the late-stage (autometasomatic) hydrous veins produced in the final cooling stages of a melt-peridotite network.

[47] Overall, these interpretations indicate that the secondary minerals that post-date the formation of the dunite protolith were produced in the uppermost mantle and not at great depths within the subduction zone by slab-derived fluids or melts. If these interpretations are correct, they imply that the xenoliths were created and modified in situ at shallow mantle levels beneath Shiveluch Volcano (<45 km), and that they may in fact be related in

some way to the genesis of magmas produced at Shiveluch.

7. Conclusions

[48] Spinel-bearing ultramafic xenoliths from Shiveluch Volcano, Kamchatka are predominantly coarse-grained and porphyroclastic harzburgite with minor occurrences of dunite, lherzolite, amphibole/phlogopite-bearing pyroxenite, and clinopyroxenite. Textures and mineral compositions suggest that the peridotites and hydrous pyroxenites were replacive dunites that formed by reactions between oxidized melts and mantle wall rock. Fibrous orthopyroxene, occurring only along olivine grain boundaries and as monomineralic veins within coarse olivine, was produced by reactions between late-stage silica-rich hydrous fluids/melts and olivine in the dunite protolith. These late-stage fluids/melts, which dissolved olivine and precipitated opx, are interpreted as the autometasomatic products of hydrous magmas that were trapped in the uppermost mantle. Veins of amphibole-phlogopite-opx appear to be the final-stage, volatile-enriched deuteric products that were created upon magma crystallization. P-T estimates are 800–1000°C and 1.03–2.21 GPa, based on two-pyroxene thermometry and Ca-in-olivine barometry, and indicate that the last equilibration of the xenoliths was just below the Moho. The xenoliths record some of the highest oxygen fugacity estimates yet described for mantle samples with fO_2 from +1.4–+2.6 ΔFMQ in peridotites and +2.4–3.3 ΔFMQ in cumulate clinopyroxenites. The high fO_2 in the Shiveluch xenoliths was likely acquired by the melt-rock reaction processes that formed the dunite protolith prior to the mineralization that formed the hydrous mineral-bearing veins and grain boundary development of opx. Thus the Shiveluch xenoliths appear to be formed and modified entirely within the uppermost mantle and not at great depths in the subduction zone by slab-derived hydrous fluids/melts or by transport of the xenoliths to the surface. This study therefore demonstrates that melt-mantle interactions at shallow levels may be a dominant process contributing to the observed high fO_2 and mineralogical variability of arc peridotites compared to abyssal and continental mantle samples.

Acknowledgments

[49] This work was funded by NSF grant EAR0310146 to G.M.Y. Thanks to A. Koloskov, G. Ponomarov, and C. Dektor for their assistance in collecting the samples used in this study. Thanks also to G. Brey and B. Wood for providing olivine and spinel microprobe standards. Helpful discussions with Peter Kelemen, Asish Basu, and Othmar Müntener significantly improved the quality of this paper and are gratefully acknowledged. Shoji Arai, Kazuhito Ozawa, and an anonymous reviewer provided thorough and thoughtful reviews. Thanks also to Vincent Salters for his efficient handling of this paper.

References

Aharonov, E., et al. (1997), Three-dimensional flow and reaction in porous media: Implications for the Earth's mantle and sedimentary basins, *J. Geophys. Res.*, *102*(B7), 14,821–14,834.

Arai, S. (1994), Characterization of spinel peridotites by olivine-spinel compositional relationships: Review and interpretation, *Chem. Geol.*, *113*, 191–204.

Arai, S., and M. Kida (2000), Origin of fine-grained peridotite xenoliths from Iraya volcano of Batan Island, Philippines: Deserpentinization or metasomatism at the wedge mantle beneath an incipient arc?, *Island Arc*, *9*, 458–471.

Arai, S., et al. (2003), Metasomatized harzburgite xenoliths from Avacha volcano as fragments of mantle wedge of the Kamchatka arc: Implications for the metasomatic agent, *Island Arc*, *12*, 233–246.

Arai, S., et al. (2004), Petrology of peridotite xenoliths from Iraya Volcano, Philippines, and its implications for dynamic mantle-wedge processes, *J. Petrol.*, *45*, 369–389.

Ballhaus, C., et al. (1991), High pressure experimental calibration of the olivine-orthopyroxene-spinel oxygen geobarometer: Implications for the oxidation state of the upper mantle, *Contrib. Mineral. Petrol.*, *107*, 27–40.

Basu, A. R. (1977), Textures, microstructures and deformation of ultramafic xenoliths from San Quintin, Baja California, *Tectonophysics*, *43*, 213–246.

Blatter, D. L., and I. S. E. Carmichael (1998), Hornblende peridotite xenoliths from central Mexico reveal the highly oxidized nature of subarc mantle, *Geology*, *26*, 1035–1038.

Bonatti, E., and P. J. Michael (1989), Mantle peridotites from continental rifts to oceanic basins to subduction zones, *Earth Planet. Sci. Lett.*, *91*, 297–311.

Boyd, F. R. (1989), Compositional distinction between oceanic and cratonic lithosphere, *Earth Planet. Sci. Lett.*, *96*, 15–26.

Brandon, A. D., and D. S. Draper (1996), Constraints on the origin of the oxidation state of mantle overlying subduction zones: An example from Simcoe, Washington, USA, *Geochim. Cosmochim. Acta*, *60*, 1739–1749.

Brey, G. P., and T. Köhler (1990), Geothermobarometry in four-phase Lherzolites II. New thermobarometers, and practical assessment of existing thermobarometers, *J. Petrol.*, *31*, 1353–1378.

Bryndzia, L. T., and B. J. Wood (1990), Oxygen thermobarometry of abyssal spinel peridotites: The redox state and C-O-H volatile composition of the Earth's sub-oceanic upper mantle, *Am. J. Sci.*, *290*, 1093–1116.

Carmichael, I. S. E. (1991), The redox states of basic and silicic magmas: A reflection of their source regions?, *Contrib. Mineral. Petrol.*, *106*, 129–141.

Chernosky, J. V., et al. (1998), The stability of tremolite: New experimental data and a thermodynamic assessment, *Am. Mineral.*, *83*, 726–739.

Conrad, W. K., and R. W. Kay (1984), Ultramafic and mafic inclusions from Adak Island: Crystallization history, and implications for the nature of primary magmas and crustal evolution in the Aleutian arc, *J. Petrol.*, *25*, 88–125.

DeBari, S., and R. G. Coleman (1989), Examination of the deep levels of an island arc: Evidence from the Tonsina ultramafic-mafic assemblage, Tonsins, Alaska, *J. Geophys. Res.*, *94*, 4373–4391.

DeBari, S. M., et al. (1987), Ultramafic xenoliths from Adagdak Volcano, Adak, Aleutian Islands, Alaska: Deformed igneous cumulates from the Moho of an island arc, *J. Geol.*, *95*, 329–341.

Dektor, C. (2006), Petrology and geochemistry of mafic and ultramafic xenoliths from Kharchinsky volcano, Kamchatka, Master's thesis, 75 pp., Univ. of S. C., Columbia.

Dektor, C. L., et al. (2005), Petrology of ultramafic xenoliths from Kharchinsky Volcano, Russia, *Geochim. Cosmochim. Acta*, suppl., *69*, A643.

Dick, H. J. B., and T. Bullen (1984), Chromian spinel as a petrogenetic indicator in abyssal and alpine-type peridotites and spatially associated lavas, *Contrib. Mineral. Petrol.*, *86*, 54–76.

Dick, H. J. B., and R. L. Fisher (1984), Mineralogic studies of the residues of mantle melting: Abyssal and alpine-type peridotites, in *Kimberlites II: The Mantle and Crust-Mantle Relationships*, edited by J. Kornprobst, pp. 295–308, Elsevier, New York.

Dick, H. J. B., et al. (1984), Mineralogic variability of the uppermost mantle along mid-ocean ridges, *Earth Planet. Sci. Lett.*, *69*, 88–106.

Draper, D. S. (1992), Spinel lherzolite xenoliths from Lorena Butte, Simcoe Mountains, southern Washington (USA), *J. Geol.*, *100*, 766–776.

Droop, G. T. R. (1987), A general equation for estimating Fe^{3+} concentrations in ferromagnesian silicates and oxides from microprobe analyses, using stoichiometric criteria, *Mineral. Mag.*, *51*, 431–435.

Ertan, I. E., and W. P. Leeman (1996), Metasomatism of Cascades subarc mantle: Evidence from a rare phlogopite orthopyroxenite xenolith, *Geology*, *24*, 451–454.

Franz, L., et al. (2002), Metasomatic mantle xenoliths from the Bismarck Microplate (Papua New Guinea)—Thermal evolution, geochemistry and extent of slab-induced metasomatism, *J. Petrol.*, *43*, 315–343.

Frey, F. A., and M. Prinz (1978), Ultramafic inclusions from San Carlos, Arizona: Petrologic and geochemical data bearing on their petrogenesis, *Earth Planet. Sci. Lett.*, *38*, 129–176.

Goto, A., and Y. Tatsumi (1990), Stability of chlorite in the upper mantle, *Am. Mineral.*, *75*, 105–108.

Greene, A. R., et al. (2006), A detailed geochemical study of island arc crust: The Talkeetna Arc section, south-central Alaska, *J. Petrol.*, *47*, 1051–1093.

Harte, B. (1977), Rock nomenclature with particular relation to deformation and recrystallization textures in olivine-bearing xenoliths, *J. Geol.*, *85*, 279–288.

Hawkesworth, C. J., et al. (1987), Isotope variations in Recent volcanics: A trace-element perspective, in *Mantle Metasomatism*, edited by M. A. Menzies and C. J. Hawkesworth, pp. 365–388, Elsevier, New York.

Herzberg, C. T. (1978), Pyroxene geothermometry and geobarometry: Experimental and thermodynamic evaluation of some subsolidus phase relations involving pyroxenes in the system CaO-MgO-Al_2O_3–SiO_2, *Geochim. Cosmochim. Acta*, *42*, 945–957.

Humphreys, M. C. S., et al. (2006), Magma evolution and open-system processes at Shiveluch Volcano: Insights from phenocryst zoning, *J. Petrol.*, *47*, 2303–2334.

Ionov, D. A., and B. J. Wood (1992), The oxidation state of subcontinental mantle: Oxygen thermobarometry of mantle xenoliths from central Asia, *Contrib. Mineral. Petrol.*, *111*, 179–193.

Ionov, D. A., et al. (1994), Metasomatism-induced melting in mantle xenoliths from Mongolia, *J. Petrol.*, *35*, 753–785.

Jaques, A. L., and D. H. Green (1980), Anhydrous melting of peridotite at 0–15 Kb pressure and the genesis of tholeiitic basalts, *Contrib. Mineral. Petrol.*, *73*, 287–310.

Jenkins, D. M. (1983), Stability and composition relations of calcic amphiboles in ultramafic rocks, *Contrib. Mineral. Petrol.*, *83*, 375–384.

Kay, R. W. (1980), Volcanic arc magma genesis: Implications for element recycling in the crust-upper mantle system, *J. Geol.*, *88*, 497–522.

Kelemen, P. B. (1990), Reaction between ultramafic rock and fractionating basaltic magma I. Phase relations, the origin of calc-alkaline magma series, and the formation of discordant dunite, *J. Petrol.*, *31*, 51–98.

Kelemen, P. B., and H. J. B. Dick (1995), Focused melt flow and localized deformation in the upper mantle: Juxtaposition of replacive dunite and ductile shear zones in the Josephine peridotite, SW Oregon, *J. Geophys. Res.*, *100*, 423–438.

Kelemen, P. B., et al. (1990), Reaction between ultramafic rock and fractionating basaltic magma II. Experimental investigation of reaction between olivine tholeiite and harzburgite at 1150–1050C and 5 kb, *J. Petrol.*, *31*, 99–134.

Kelemen, P. B., et al. (1995a), Extraction of mid-ocean-ridge basalt from the upwelling mantle by focused flow of melt in dunite channels, *Nature*, *375*, 747–753.

Kelemen, P. B., et al. (1995b), Experiments on flow focusing in soluble porous media, with applications to melt extraction from the mantle, *J. Geophys. Res.*, *100*, 475–496.

Kelemen, P. B., et al. (2003), Thermal structure due to solid-state flow in the mantle wedge beneath arcs, in *Inside the Subduction Factory*, *Geophys. Monogr. Ser.*, vol. 138, edited by J. Eiler, pp. 293–311, AGU, Washington, D. C.

Kepezhinskas, P., and M. J. Defant (1996), Contrasting styles of metasomatism above subduction zones: Constraints from ultramafic xenoliths in Kamchatka, in *Subduction Top to Bottom*, *Geophys. Monogr. Ser.*, vol. 96, edited by G. E. Bebout et al., pp. 307–314, AGU, Washington, D. C.

Köhler, T., and G. P. Brey (1990), Calcium exchange between olivine and clinopyroxene calibrated as a geothermobarometer for natural peridotites from 2 to 60 kb with applications, *Geochim. Cosmochim. Acta*, *54*, 2375–2388.

Koloskov, A. V., and M. Y. Khotin (1978), Ultramafic inclusions in lavas of present Kamchatka volcanoes, in *Inclusions in the Volcanic Rocks of the Kuril-Kamchatka Island Arc* (in Russian), pp. 36–66, Nauka, Moscow.

Konstantinovakaia, E. A. (2000), Geodynamics of an early Eocene arc-continent collision reconstructed from the Kamchatka Orogenic Belt, NE Russia, *Tectonophysics*, *325*, 87–105.

Leake, B. E., et al. (1997), Nomenclature of amphiboles: Report of the Subcommittee on Amphiboles of the International Mineralogical Association, Commission on New Minerals and Mineral Names, *Am. Mineral.*, *82*, 1019–1037.

Levin, V., et al. (2002), Crust and upper mantle of Kamchatka from teleseismic receiver functions, *Tectonophysics*, *358*, 223–265.

Luhr, J. F., and J. J. Aranda-Gomez (1997), Mexican peridotite xenoliths and tectonic terranes: Correlations among vent location, texture, temperature, pressure, and oxygen fugacity, *J. Petrol.*, *38*, 1075–1112.

Maury, R. C., et al. (1992), Metasomatism of the sub-arc mantle inferred from trace elements in Philippine xenoliths, *Nature*, *360*, 661–663.

McInnes, B., et al. (2001), Hydrous metasomatism of oceanic sub-arc mantle, Lihir, Papua New Guinea: Petrology and geochemistry of fluid-metasomatized mantle wedge xenoliths, *Earth Planet. Sci. Lett.*, *188*, 169–183.

McKenzie, D. (1985), The extraction of magma from the crust and mantle, *Earth Planet. Sci. Lett.*, *74*, 81–91.

Melekestsev, I. V., et al. (1991), Sheveluch Volcano, in *Active Volcanoes of Kamchatka*, edited by S. A. Fedotov and Y. P. Masurenkov, pp. 98–103, Nauka, Moscow.

Mercier, J. C., and A. Nicolas (1975), Textures and fabrics of upper-mantle peridotites as illustrated by xenoliths from basalt, *J. Petrol.*, *16*, 454–487.

Mungall, J. E. (2002), Roasting the mantle: Slab melting and the genesis of major Au and Au-rich Cu deposits, *Geology*, *30*, 915–918.

Obata, M., et al. (1974), The iron-magnesium partitioning between naturally occurring coexisting olivine and Ca-rich clinopyroxene: An application of the simple mixture model to olivine solid solution, *Bull. Soc. Fr. Mineral. Cristallogr.*, *97*, 101–107.

O'Neill, H. S. (1981), The transition between spinel lherzolite and garnet lherzolite, and its use as a geobarometer, *Contrib. Mineral. Petrol.*, *77*, 185–194.

O'Neill, H. S., and V. J. Wall (1987), The olivine-orthopyroxene-spinel oxygen geobarometer, the nickel precipitation curve, and the oxygen fugacity of the earth's upper mantle, *J. Petrol.*, *28*, 1169–1191.

Ozawa, K. (1983), Evaluation of olivine-spinel geothermometry as an indicator of thermal history for peridotites, *Contrib. Mineral. Petrol.*, *85*, 52–65.

Ozawa, K. (1994), Melting and melt segregation in the mantle wedge above a subduction zone: Evidence from the chromite-bearing peridotites of the Miyamori ophiolite complex, northeastern Japan, *J. Petrol.*, *35*, 647–678.

Parkinson, I. J., and R. J. Arculus (1999), The redox state of subduction zones: Insights from arc-peridotites, *Chem. Geol.*, *160*, 409–423.

Parkinson, I. J., and J. A. Pearce (1998), Peridotites from the Izu-Bonin-Mariana Forearc (ODP Leg 125): Evidence for mantle melting and melt-mantle interaction in a supra-subduction zone setting, *J. Petrol.*, *39*, 1577–1618.

Parkinson, I. J., et al. (2003), Peridotite xenoliths from Grenada, Lesser Antilles Island Arc, *Contrib. Mineral. Petrol.*, *146*, 241–262.

Pawley, A. (2003), Chlorite stability in mantle peridotite: The reaction clinchlore + enstatite = forsterite + pyrope + H_2O, *Contrib. Mineral. Petrol.*, *144*, 449–456.

Perfit, M. R., et al. (1980), Chemical characteristics of island-arc basalts: Implications for mantle sources, *Chem. Geol.*, *30*, 227–256.

Plank, T., and C. H. Langmuir (1993), Tracing trace elements from sediment input to volcanic output at subduction zones, *Nature*, *362*, 739–742.

Polyak, B. G., and I. V. Melekestsev (1981), Production rate of volcanoes (in Russian), *Volcanol. Seismol.*, *5*, 22–37.

Prouteau, G., et al. (2001), Evidence for mantle metasomatism by hydrous silicic melts derived from subducted oceanic crust, *Nature*, *410*, 197–200.

Quick, J. E. (1981), The origin and significance of large, tabular dunite bodies in the Trinity peridotite, Northern California, *Contrib. Mineral. Petrol.*, *78*, 413–422.

Ringwood, A. E. (1974), The petrological evolution of island arc systems, *J. Geol. Soc. London*, *130*, 183–204.

Schiano, P., et al. (1995), Hydrous, silica-rich melts in the sub-arc mantle and their relationship with erupted arc lavas, *Nature*, *377*, 595–600.

Smith, D., and J. C. A. Riter (1997), Genesis of evolution of low-Al orthopyroxene in spinel peridotite xenoliths, Grand Canyon field, Arizona, USA, *Contrib. Mineral. Petrol.*, *127*, 391–404.

Streckeisen, A. (1979), Classification and nomenclature of volcanic rocks, lamprophyres, carbonatites, and melilitic rocks: Recommendations and suggestions of the IUGS subcommission on the systematics of igneous rocks, *Geology*, *7*, 331–335.

Takahashi, E. (1980), Thermal history of lherzolite xenoliths: I. Petrology of lherzolite xenoliths from Ichinomegata crater, Oga peninsula, northeast Japan, *Geochem. Cosmochim. Acta*, *44*, 1643–1658.

Tatsumi, Y., et al. (1986), Chemical characteristics of fluid phase released from a subducted lithosphere and origin of arc magmas: Evidence from high-pressure experiments and natural rocks, *J. Volcanol. Geotherm. Res.*, *29*, 293–309.

Toramaru, A., and N. Fujii (1986), Connectivity of melt phase in a partially molten peridote, *J. Geophys. Res.*, *91*, 9239–9252.

Trommsdorff, V., et al. (1998), High pressure breakdown of antigorite to spinifex-textured olivine and orthopyroxene, SE Spain, *Contrib. Mineral. Petrol.*, *132*, 139–148.

van Keken, P. E., et al. (2002), High-resolution models of subduction zones: Implications for mineral dehydration reactions and the transport of water into the deep mantle, *Geochem. Geophys. Geosyst.*, *3*(10), 1056, doi:10.1029/2001GC000256.

von Bargen, N., and H. S. Waff (1986), Permeabilities, interfacial areas and curvatures of partially molten systems: Results of numerical computations of equilibrium microstructures, *J. Geophys. Res.*, *91*, 9261–9276.

von Seckendorff, V., and H. O'Neill (1993), An experimental study of F-Mg partitioning between olivine and orthopyroxene at 1173, 1273 and 1423 K and 1.6 GPa, *Contrib. Mineral. Petrol.*, *113*, 196–207.

Wager, L. R., and G. M. Brown (1967), *Layered Igneous Rocks*, W. H. Freeman, New York.

Wilson, A. H. (1982), The geology of the Great 'Dyke', Zimbabwe: The ultramafic rocks, *J. Petrol.*, *23*, 240–292.

Wood, B. J., and D. Virgo (1989), Upper mantle oxidation state: Ferric iron contents of lherzolite spinels by ^{57}Fe Mössbauer spectroscopy and resultant oxygen fugacities, *Geochim. Cosmochim. Acta*, *53*, 1277–11291.

Wood, B. J., et al. (1990), Mantle oxidation state and its relationship to tectonic environment and fluid speciation, *Science*, *248*, 337–345.